



HAL
open science

Leptin brain entry via a tanycytic LepR–EGFR shuttle controls lipid metabolism and pancreas function

Manon Duquenne, Cintia Folgueira, Cyril Bourouh, Marion Millet, Anisia Silva, Jérôme Clasadonte, Monica Imbernon, Daniela Fernandois, Ines Martinez-Corral, Soumya Kusumakshi, et al.

► To cite this version:

Manon Duquenne, Cintia Folgueira, Cyril Bourouh, Marion Millet, Anisia Silva, et al.. Leptin brain entry via a tanycytic LepR–EGFR shuttle controls lipid metabolism and pancreas function. *Nature Metabolism*, 2021, 3 (8), pp.1071-1090. 10.1038/s42255-021-00432-5 . hal-03365135

HAL Id: hal-03365135

<https://hal.science/hal-03365135v1>

Submitted on 5 Oct 2021

HAL is a multi-disciplinary open access archive for the deposit and dissemination of scientific research documents, whether they are published or not. The documents may come from teaching and research institutions in France or abroad, or from public or private research centers.

L'archive ouverte pluridisciplinaire **HAL**, est destinée au dépôt et à la diffusion de documents scientifiques de niveau recherche, publiés ou non, émanant des établissements d'enseignement et de recherche français ou étrangers, des laboratoires publics ou privés.

1 Submission: April 2, 2021

2 *Nature Metabolism*

3 Research Article

4

5 **Leptin enters the brain through a LepR:EGFR shuttle in tanycytes to** 6 **regulate peripheral lipogenesis and pancreatic β -cell function**

7

8 **Manon Duquenne¹, Cintia Folgueira^{2#}, Cyril Bourrouh^{3#}, Marion Millet^{4,#}, Anisia Silva^{5#},**
9 **Jérôme Clasadonte^{1#}, Monica Imbernon¹, Daniela Fernandois¹, Ines Martinez-Corral¹,**
10 **Soumya Kusumakshi⁶, Emilie Caron¹, S. Rasika¹, Eleonora Deliglia¹, Nathalie Jouy^{1,12},**
11 **Asturo Oishi⁵, Massimiliano Mazzone⁷, Eric Trinquet⁸, Jan Tavernier⁹, Young-Bum Kim¹¹,**
12 **Stéphane Ory⁴, Ralf Jockers⁵, Markus Schwaninger¹⁰, Ulrich Boehm⁶, Ruben Nogueiras²,**
13 **Jean-Sébastien Annicotte³, Stéphane Gasman^{4&}, Julie Dam^{5&}, Vincent Prévot^{1&*}**

14

15 ¹ Univ. Lille, Inserm, CHU Lille, Laboratory of Development and Plasticity of the Neuroendocrine Brain,
16 Lille Neuroscience & Cognition, UMR_S1172, EGID, DISTALZ, F-59000 Lille, France

17 ² CIMUS, Universidade de Santiago de Compostela-Instituto de Investigación Sanitaria, Santiago de
18 Compostela, 15782, Spain- CIBER Fisiopatología de la Obesidad y Nutrición (CIBERObn), 15706,
19 Spain

20 ³ Univ. Lille, Inserm, CHU Lille, Institut Pasteur de Lille, CNRS, U1283 - UMR 8199 - EGID, F-59000
21 Lille, France

22 ⁴ Centre National de la Recherche Scientifique, Université de Strasbourg, Institut des Neurosciences
23 Cellulaires et Intégratives, F-67000 Strasbourg, France.

24 ⁵ Institut Cochin, Inserm U1016, CNRS UMR 8104, University Paris Descartes, Sorbonne Paris Cité,
25 Paris, France

26 ⁶ Experimental Pharmacology, Center for Molecular Signaling (PZMS), Saarland University School of
27 Medicine, 66421, Homburg, Germany

28 ⁷ Laboratory of Tumor Inflammation and Angiogenesis, Center for Cancer Biology, VIB, Department of
29 Oncology, KU Leuven, Leuven, B3000, Belgium

30 ⁸ Cisbio Bioassays, Parc Technologique Marcel Boiteux, BP84175, F-30200 Codolet, France

31 ⁹ VIB-UGent Center for Medical Biotechnology, Gent, Belgium.

32 ¹⁰ Institute for Experimental and Clinical Pharmacology and Toxicology, University of Lübeck, Lübeck,
33 Germany

34 ¹¹ Division of Endocrinology, Diabetes, and Metabolism, Beth Israel Deaconess Medical Center and
35 Harvard Medical School, Boston, MA, USA.

36 ¹² Flow core Facility, Bioluminescence Imaging Center of Lille, campus HU, UMS2014-US41, F-59000 Lille, France

37

38

39 [#] These authors contributed equally to this work

40 [&] These authors jointly supervised this work

41

42 Running Title: Tanycytes are conduits for peripheral metabolic signals into the brain

43 * Corresponding author: Vincent Prevot, Ph.D., Inserm 1172, Bâtiment Biserte,
44 Place de Verdun, 59045 Lille Cedex, France

45 Tel : +33 612-90-38-76

46 Fax : +33 320-53-85-62

47 E-mail : vincent.prevot@inserm.fr

48

49

50 Number of text pages: 53

51 Number of figures: 7

52 Number of Supplementary Figures: 7

53 Number of tables: 0

54 Number of words (abstract): 150

55 Number of words (Text): 7290

56

57

58

59 **SUMMARY**

60 Metabolic health depends on the brain's ability to control food intake and nutrient use versus storage,
61 processes that require peripheral signals such as the adipocyte-derived hormone, leptin, to cross brain
62 barriers and mobilize regulatory circuits. We have previously shown that hypothalamic tanycytes shuttle
63 leptin into the brain to reach target neurons. Here, using multiple complementary models, we show that
64 tanycytes express functional leptin receptor (LepRb), respond to leptin by triggering Ca²⁺ waves and
65 target-protein phosphorylation, and that their transcytotic transport of leptin requires the activation of a
66 LepR:EGFR complex by leptin and EGF sequentially. Selectively deleting LepR in tanycytes blocks leptin
67 entry into the brain, inducing not only increased food intake and lipogenesis but glucose intolerance
68 through attenuated insulin secretion by pancreatic β -cells, possibly via altered sympathetic nervous tone.
69 Tanycytic LepRb:EGFR-mediated transport of leptin could thus be crucial to the pathophysiology of
70 diabetes in addition to obesity, with therapeutic implications.

71

72

73 **INTRODUCTION**

74
75 Type 2 diabetes (T2D) is a common multigenic disorder affecting almost 10% of the world's population
76 ¹. However, the characteristics of this disorder do not appear to be homogeneous across the globe. In
77 Asia, for example, TD2 develops in a much shorter time, in a younger age group, and in people with a
78 much lower body-mass index (BMI) than in patients from other parts of the globe ². In addition, while
79 Asian population studies suggest that a decrease in insulin production by β -cells is crucial for the
80 development of diabetes, impaired insulin sensitivity, i.e. the ability to modulate glucose levels in
81 response to circulating insulin, appears to be a prerequisite for incident diabetes in other ethnicities,
82 including Europeans ^{2,3}.

83 Leptin is a 16-kDa peptide hormone produced by adipocytes. It functions as an afferent signal in a
84 negative feedback loop that not only controls feeding and maintains energy homeostasis ⁴⁻⁹, but also
85 regulates glucose metabolism ^{10,11} and substrate fluxes ^{12,13} by activating leptin receptor (LepR)
86 signaling in the brain. How circulating leptin is transported into the central nervous system to reach its
87 target neurons remains an enigma. However, an increasing body of evidence points to the median
88 eminence, a circumventricular organ in the basal hypothalamus adjacent to the arcuate nucleus
89 (ARH), as a key entrance point for leptin into the metabolic brain ¹⁴⁻¹⁶.

90 By virtue of the fenestrated or porous endothelium of the underlying pituitary portal blood vessels,
91 which replaces a traditional blood-brain barrier (BBB), the median eminence acts as a brain window at
92 which circulating signals, including metabolic hormones, may enter the brain by passive diffusion ^{17,18}.
93 Among the neuronal populations responsive to metabolic hormones in this region, those of the
94 ventromedial ARH (vmARH) ^{17,19} and neurons that extend dendrites into the median eminence can
95 directly sense this local blood-borne information ²⁰. However, the passive diffusion of metabolic signals
96 into the median eminence is limited in extent ^{17,19}, and tanycytes, a specialized glial cell type lining the
97 floor of the third ventricle (3V), form a blood-cerebrospinal-fluid (CSF) barrier that prevents these
98 circulating metabolic signals from reaching deeper hypothalamic structures through the CSF ¹⁴⁻¹⁶.
99 Consequently, in order to reach more distant targets such as neurons of the dorsomedial ARH
100 (dmARH), these signals require an active transport mechanism to cross the tanycytic blood-CSF
101 barrier ^{21,22}.

102 In a previous study, we have shown that tanycytes, whose end-feet contact the fenestrated
103 capillaries of the median eminence, themselves internalize and shuttle blood-borne leptin

104 extravasating from these fenestrations into the CSF, in an ERK-dependent manner²³. However, the
105 putative involvement of LepR in this transcytotic transport process has remained unclear, with some
106 authors questioning the expression of LepR by tanycytes^{24,25}.

107 Here, by employing multiple *in vitro* and *in vivo* approaches and several mouse models, we
108 demonstrate that tanycytes do indeed express functional LepR, and that this LepR expression is
109 required for the transcytotic transport of peripheral leptin into the CSF, a process that appears to play
110 a vital role in the central control of pancreatic β -cell function, lipid accumulation and subsequent
111 glucose homeostasis.

112

113 **RESULTS**

114 **LepR is expressed and active in tanycytes of the median eminence**

115 In order to verify the expression of LepR by median eminence and ARH tanycytes, we first used
116 the powerful RNAscope approach with probes targeting the long and short forms of LepR, LepRb and
117 LepRa, respectively. Interestingly, while both isoforms were present in tanycytic cell bodies lining the
118 walls of the 3V, this expression was relatively weak compared to the overwhelmingly high expression
119 seen in leptin-responsive neurons of the ARH, providing an explanation for the failure of other, less
120 sensitive, methods to detect tanycytic LepR expression without resorting to the isolation of these cells
121 (Supplementary Figure 1A). We therefore searched for other tools such as novel antibodies capable of
122 reliably detecting LepR protein in order to confirm its presence in median eminence tanycytes. We
123 characterized the recently described biologically active allosteric antibody XPA, which was developed
124 to target mouse LepR²⁶. Using isolated parts/fragments of the LepR extracellular domain (ECD), we
125 found that the epitope specifically targeted by XPA lies in the cytokine receptor homology 1 (CRH1)
126 domain of mouse LepR (Figure 1A; Supplementary Figure 1B), outside the orthosteric leptin-binding
127 site of the CRH2 domain (Figure 1A, 1B). The use of LepR BRET biosensors indicated that XPA was
128 capable of inducing conformational changes and the oligomerization of LepR, even though these
129 changes were different from the ones promoted by the natural ligand (Figure 1C). Similarly to leptin
130 (50nM), treatment with 100nM XPA consistently triggered STAT3 signaling in HEK293, N46, HeLa and
131 CHO cells transfected with LepRb (Figure 1D; Supplementary Figure 1C), as well as ERK signaling in
132 HEK293 cells (Figure 1D). XPA also induced the phosphorylation of STAT3 in primary cultures of
133 tanycytes (Figure 1E), which we have previously shown to express LepR and to internalize

134 fluorescently labeled leptin *in vitro*²³. This indicates that, rather than simply being a passive marker of
135 LepR protein expression, XPA is also a vital marker for activated and internalized LepR. Accordingly,
136 a 5 min co-application of fluorescent leptin (125nM) and fluorescent XPA (30nM) to primary tanycyte
137 cultures showed that 100% of the cells that internalized fluorescent leptin also internalized fluorescent
138 XPA, and that 50 to 60% of the endocytosed leptin colocalized with XPA *in vitro* (Figure 1F), indicating
139 that these cells expressed LepR and internalized it in response to leptin binding. To confirm that
140 tanycytes also express LepR *in vivo*, we intravenously administered XPA (2 nmol/animal) or vehicle to
141 mice 2 min before sacrifice. At this short interval, XPA was seen to colocalize with the vimentin-
142 immunoreactive cell bodies and processes of tanycytes arching down to the fenestrated capillary
143 plexus of the median eminence (Figure 1G).

144 In our quest for further indisputable evidence of LepR expression and function in median eminence
145 tanycytes, we assessed whether tanycytes in living brain slices could respond to leptin and initiate
146 Ca²⁺ signaling, as hypothalamic neurons do^{27,28}. To selectively target tanycytes, we generated mice
147 expressing the GCamp3 calcium biosensor under the control of the *Trmp5* promoter, which is
148 selectively expressed in tanycytes in the median eminence and present in the majority of this cell
149 population (Figure 1H)²⁹, by crossing *Trmp5::Cre* mice with those allowing Cre-dependent expression
150 of GCamp3. Puffing 6 μM leptin onto the ventricular wall of brain slices against the flow of perfusion
151 resulted in a [Ca²⁺]_i increase in the cell bodies of median eminence tanycytes, as seen using live
152 imaging (Figure 1H, and 1I). A bath-application of 6 μM of the point-mutated leptin LAN
153 (L39A/D40A/F41A), which acts as a competitive antagonist by binding LepR but blocking its activity³⁰,
154 prior to puffing leptin onto tanycytes inhibited the leptin-induced [Ca²⁺]_i increase in these cells (Figure
155 1I, and 1K), suggesting that LepR activation is required for this signaling cascade. To further test the
156 actual involvement of LepR in this process, we generated mice in which LepR was selectively knocked
157 out in cells expressing the *Trmp5* promoter. In these *Trmp5::Cre; LepR^{loxP/loxP}; GCamp3^{loxP/STOP/loxP}*
158 mice (*Gcamp3^{Trmp5}*; *LepR^{Trmp5KO}* mice), puffs of leptin failed to promote any change in [Ca²⁺]_i in
159 tanycytes (Figure 1J, and 1K). However, puffs of 10 mM ATP, a well-known and potent activator of
160 calcium waves in tanycytes^{31,32}, readily elevated [Ca²⁺]_i in both LAN-treated and mutated brain slices,
161 showing the viability of the cells (Figure 1L, Supplementary Figure 2). Together, these data
162 unequivocally show that tanycytes *in vivo* express active LepR, which mediates leptin-induced
163 changes in [Ca²⁺]_i.

164

165 **EGFR-mediated LepRb signaling is required for the transcellular trafficking of leptin in**
166 **tanycytes**

167 To characterize the mechanism by which tanycytes transport blood-borne leptin into the CSF and the
168 rest of the hypothalamus, we next studied the transcytotic route followed by fluorescent leptin using
169 primary cultures of tanycytes. As early as 2 min after the internalization of fluorescent bioactive leptin,
170 the fluorescent signal was detected in EEA1-immunoreactive early endosomes (Figure 2A), where it
171 accumulated for the first 10 min. The fluorescent leptin then exited this subcellular compartment, as
172 indicated by the subsequent decrease in intensity and extinction of fluorescence over time (Figure 2B,
173 Figure 2C, Supplementary Figure 3A), along with leptin release into the culture medium (Figure 2D).
174 Similarly, fluorescent LAN, which binds to but is unable to activate LepR, was also seen to be
175 internalized (Supplementary Figure 3B) and to reach early endosomes (Supplementary Figure 3D).
176 However, the overall intensity of LAN fluorescence inside the cell remained constant over time
177 (Supplementary Figure 3B), and LAN was seen to remain sequestered in EEA1-immunoreactive
178 compartments (Figure 2E, Supplementary Figure 3C-D), suggesting that, in contrast to bioactive
179 leptin, captured LAN could not be released from tanycytes. These results suggest that LepR signaling
180 is not required for leptin uptake, but is required for internalized leptin to complete its transcytotic route
181 across tanycytes into the CSF.

182 Next, since this transcytosis could be mediated by the leptin signaling cascade, characterized by
183 the rapid activation of a series of tyrosine kinases (TK) and serine/threonine protein kinases (STK), we
184 performed kinome profiling to explore differential global kinase activity in tanycytes in the presence or
185 absence of 125nM leptin for 2, 5, 10 and 15 min. We used the PamGene array, which consists of 140
186 immobilized tyrosine- and serine/threonine-containing peptides that are the targets of most known
187 kinases (TK and STK PamChips). Peptides whose phosphorylation varied significantly between
188 control and leptin-treated primary tanycytes indicated the putative activation of specific kinases in
189 response to leptin. This kinase analysis revealed the significant activation of the EGFR pathway 2 min
190 after leptin treatment (Figure 2F) and of MAP kinases, including ERK, 2 15 min after leptin treatment
191 (Supplementary Figure 3E). We have previously reported that ERK activation is required for the
192 release of leptin internalized by tanycytes *in vitro*, and that the alteration of blood-borne leptin shuttling
193 into the hypothalamus in diet-induced obese mice can be rescued by activating ERK using potent

194 inducers such as EGF²³. Here, the novel and unexpected finding that EGFR itself is *trans*-activated by
195 leptin in tanycytes suggests a possible molecular pathway underlying our previous observations.

196 *In vivo*, EGFR immunoreactivity was detected both in the cell bodies of tanycytes lining the walls
197 and floor of the 3V and in their distal processes, which contact fenestrated capillaries at the pial
198 surface of the brain in the external zone of the median eminence (Supplementary Figure 4A).
199 Polymerase ligation assays using XPA demonstrated the extensive physical interaction of EGFR and
200 LepRb in both cellular compartments, a phenomenon that is blunted in *Trmp5::Cre; LepR^{loxP/loxP}* mice
201 (Figure 2G), suggesting that LepRb:EGFR signaling in tanycytic end-feet may play a role in the
202 transcellular transport of circulating leptin once it is captured from the bloodstream.

203 We then explored this interaction between EGFR and LepR signaling. Co-transfection experiments
204 in HEK293 cells confirmed that EGFR was immunoprecipitated with LepR, suggesting, intriguingly,
205 that the two receptors could physically interact with each other even in the absence of a ligand (Figure
206 2H). To study the effect of ligand binding on this interaction, we next used Time-Resolved
207 Fluorescence Resonance Energy Transfer (TR-FRET) in living HEK293 cells to investigate the
208 proximity between leptin and EGF and their cognate receptors within the LepR:EGFR complex
209 (Supplementary Figure 3F). Taking advantage of targeted fluorescently-labeled SNAP receptors
210 (energy donor, Terbium (**Tb**)) and ligands (labeled with the energy acceptor, **d2**), TR-FRET enables
211 the demonstration of the proximity of a ligand at a distance of 10 nm or less to a specific and unique
212 receptor within a heteromeric receptor complex³³. Because leptin does not bind to EGFR, the
213 incubation of fluorescent leptin-d2 even at high concentrations with fluorescently labeled SNAP-EGFR
214 did not lead to any TR-FRET signal (Figure 2I, Supplementary Figure 3F). However, the co-expression
215 of unlabeled LepR in fluorescent SNAP-EGFR-expressing cells in the presence of leptin-d2 gave rise
216 to a significant and specific TR-FRET signal, demonstrating the close proximity between SNAP-EGFR,
217 LepR and leptin-d2 (Figure 2I, Supplementary Figure 3F). This binding of leptin-d2 to the SNAP-
218 EGFR:LepR complex was seen to increase and to reach saturation in a concentration-dependent
219 manner, with an affinity ($K_D(\text{SNAP-EGFR:LepRb}) = 0.42 [0.26-0.49] \text{ nM}$) similar to the affinity of leptin
220 binding to isolated LepR³⁴ (Figure 2I). EGF binding to EGFR did not modify the affinity of leptin
221 binding to the LepR:EGFR complex (Figure 2I), but the significantly higher Bmax of the saturation
222 curve indicates that it likely induced a conformational change in LepR within the molecular complex
223 (Figure 2I; Supplementary Figure 3G). Similarly, cells expressing EGFR and fluorescent SNAP-LepR

224 that were stimulated by EGF-d2 (Supplementary Figure 3H) were seen to emit a specific TR-FRET
225 signal, reflecting the interaction between SNAP-LepR:EGFR:EGF-d2 (Supplementary Figure 3I). A
226 weak TR-FRET signal detected between SNAP-LepR and EGF-d2 in the absence of heterologous
227 EGFR may have arisen from a weak interaction between SNAP-LepR and endogenous EGFR. As
228 suggested by the model fitting of the saturation curve, EGF-d2 interacted with EGFR within the
229 LepR:EGFR complex with the same affinity ($K_D(\text{SNAP-LepRb:EGFR}) = 2.1 [1.6-2.5] \text{ nM}$) as with
230 isolated EGFR alone ($K_D(\text{SNAP-EGFR}) = 3.2 [2.4-3.7]$) (Supplementary Figure 3J). In line with the
231 binding of leptin-d2 or EGF-d2 to their cognate receptors within the complex, the proximity of
232 fluorescent leptin-Tb (energy donor) to EGF-d2 (energy acceptor) was only detected when both LepR
233 and EGFR were co-expressed (Supplementary Figure 3K, 3L), suggesting the formation of a
234 quaternary complex, Leptin:LepR:EGFR:EGF, in these cells.

235 In isolated tanycytes, combined treatment with leptin and EGF enhanced EGFR and ERK
236 phosphorylation, supporting the intricate collaboration between these two receptors at the level of the
237 tanycytic ERK signaling pathway (Figure 2J). Accordingly, EGF potentiated the leptin:LepR activation
238 of the ERK signaling pathway in HEK293T cells, a reaction that was blunted by pre-treating the cells
239 with the EGFR kinase inhibitor, AG1478 (Figure 2K). Conversely, the inhibition of MEK1/2, the
240 upstream activators of ERK, using U0126 led to the accumulation of fluorescent leptin in EAA1-
241 immunoreactive early endosomes in tanycytes and blunted its release (Figure 2D), thus phenocopying
242 the behavior of fluorescent LAN, which does not activate LepR, after its internalization by tanycytes
243 (Figure 2E, Supplementary Figure 3B, 3C, 3D). We next verified whether this lack of LAN release from
244 the early endosome compartment in tanycytes could be bypassed by directly activating the EGFR-
245 ERK signaling pathway. EGF treatment (1.5nM) strikingly restored the trafficking of fluorescent LAN
246 downstream of early endosomes (Figure 2E) and its probable release by tanycytes, suggesting that
247 EGFR activation occurs downstream of LepR activation (Supplementary Figure 3C). Together, these
248 data indicate that the transcytosis of leptin by tanycytes, which allows it to reach the CSF and distant
249 hypothalamic tissues, requires LepR-EGFR-ERK signaling.

250

251 **Mice lacking LepR-EGFR signaling in adult tanycytes show increased fat mass gain linked to**
252 **restricted access of blood-borne leptin to the hypothalamus**

253 To examine the functional role of LepR expression in adult tanycytes, we used the injection of the
254 TAT-Cre recombinant protein into the 3V of *LepR*^{loxP/loxP} mice. The use of *tdTomato*^{loxP-STOP-loxP} reporter
255 mice revealed that 2 μ l TAT-Cre infusion into the 3V (1.27 μ g/ μ l over 15 min) caused genetic
256 recombination in about 60% of the tanycytes of the median eminence (Supplementary Figure 5A and
257 5B), but not in tanycytes of the area postrema, another circumventricular organ in the brainstem
258 involved in the regulation of energy homeostasis³⁵ (Supplementary Figure 5C). In contrast, TAT-Cre
259 infusion into the fourth ventricle (4V) was seen to target both median eminence and area postrema
260 tanycytes (Supplementary Figure 5C), while TAT-Cre infusion into the lateral ventricle was ineffective
261 in inducing Tomato expression in median eminence tanycytes (Supplementary Figure 5A - 5B). FACS
262 isolation of Tomato-positive ependymal cells from microdissected dorsal and ventral aspects of the
263 3V, which are enriched in ciliated ependymal cells and tanycytes, respectively (Supplementary Figure
264 5D), showed that LepR expression was readily detected by real-time PCR in the tanycyte-enriched
265 population, but not in classical ependymal cells (Supplementary Figure 5E). Accordingly, FACS
266 isolation of Tomato-positive median eminence tanycytes after the infusion of TAT-Cre into the 3V of
267 *tdTomato*^{loxP-STOP-loxP}; *LepR*^{loxP/loxP} mice (Figure 3A) showed that the expression of transcripts encoding
268 both the short forms of LepR as well as LepRb was significantly diminished in these cells, when
269 compared to Tomato-positive tanycytes from *tdTomato*^{Tan}; *LepR*^{+/+} mice (Figure 3B and 3C).
270 Interestingly, the transcript of *Socs3*, a known leptin-responsive transcriptional target³⁶, was also
271 found to be downregulated in Tomato-positive cells from *tdTomato*^{Tan}; *LepR*^{TanKO} mice (Figure 3D).
272 Importantly, *LepR* and *Socs3* mRNA levels were not downregulated in Tomato-negative cells (Figure
273 3B-3D). The TAT-Cre-mediated loss of *LepR* expression in tanycytes was also accompanied by a
274 dramatic decrease in the PLA signal reporting the physical association between LepRb and EGFR
275 (Figure 2G), as seen in *Trmp5::Cre*; *LepR*^{loxP/loxP} mice.

276 Interestingly, mice lacking LepR in tanycytes of the median eminence were seen to eat more
277 (Supplementary Figure 6A), specifically in the morning after lights-on (Figure 3E). They also gained
278 significantly more weight (Figure 3F) than both vehicle-injected control littermates with normal
279 tanycytic LepR expression and TAT-Cre-injected heterozygous mice (*LepR*^{TanHet}). This weight gain
280 was associated with a 3-fold increase in fat mass 12 weeks after *LepR* was knocked out in tanycytes
281 (Figure 3G), with a concomitant loss of lean mass (Figure 3H) such that the net gain in body mass
282 remained moderate (Supplementary Figure 6B). At 12 weeks post-TAT-Cre injection, *LepR*^{TanKO} mice

283 showed a significant increase in visceral (Figure 3I), but not subcutaneous fat mass (Figure 3J) when
284 compared to vehicle-injected $LepR^{loxP/loxP}$ littermates. Surprisingly, this weight gain was independent of
285 hyperphagia, since $LepR^{TanKO}$ mice pair-fed with controls gained the same weight as $LepR^{TanKO}$ mice
286 fed *ad libitum* (Figure 3K and 3L). To characterize the reason for this change in body weight, we
287 monitored these mice using an indirect calorimetry system. Weight gain in $LepR^{TanKO}$ mice was
288 associated with an increased respiratory exchange ratio (RER) during the light phase both at 4 weeks
289 (Supplementary Figure 6A2) and 12 weeks after TAT-Cre injection (Figure 3M and 3N), a
290 phenomenon that was conserved under the pair-fed condition (Figure 3K), in which $LepR^{TanKO}$ mice
291 kept gaining more weight than $LepR^{loxP/loxP}$ littermates (Figure 3L), even though energy expenditure
292 (Supplementary Figure 6A3 and 6C) and locomotor activity (Supplementary Figure 6A4 and 6D)
293 remained unchanged. These phenomena were reproduced when tanycytes *in vivo* were transduced
294 with a viral vector expressing Cre under the control of the tanycyte-specific *Dio2* promoter³¹, as an
295 alternative to TAT-Cre infusion into the 3V (Supplementary Figure 6A5-A8).

296 Interestingly, in accordance with the marked increase in fat mass, circulating levels of leptin were
297 seen to be increased as early as 4 weeks after the TAT-Cre-mediated *LepR* deletion in tanycytes
298 (Figure 3O). Taking into account the close relationship between *LepR* and *EGFR* and the likely *trans-*
299 *activation* of *LepR* to some extent by endogenous EGF (Figure 2, Supplementary Figure 3), we
300 therefore also measured EGF levels in the blood of $LepR^{TanKO}$ mice, to determine whether the lack of
301 *LepR* signaling in these mice would give rise to compensatory changes in the EGF-*EGFR* signaling
302 pathway. Interestingly, we found that EGF levels, which we could readily detect in the circulation, were
303 increased in $LepR^{TanKO}$ mice (Figure 3P). However, EGF levels were unchanged in wild-type mice
304 given a high-fat diet for 8 weeks as compared to chow-fed controls (Figure 3Q), suggesting that the
305 increase in EGF levels in $LepR^{TanKO}$ mice were not related to the higher circulating leptin levels
306 observed in these animals per se (Figure 3O), but rather to central phenomena linked to deficient
307 *LepR* signaling.

308 Increased food intake after overnight feeding (Figure 3E) despite elevated adiposity (Figure 3G and
309 3I) and circulating levels of leptin in $LepR^{TanKO}$ mice (Figure 3O) further raised the possibility that these
310 animals could be developing hypothalamic resistance to circulating leptin, linked to defective leptin
311 transport across the BBB into the CSF by tanycytes, as seen at early stages of diet-induced obesity in
312 various animal models^{23,37}. First, to confirm that this phenomenon occurs under physiological

313 conditions, we assessed endogenous STAT3 activation in the ARH, which has previously been shown
314 to be linked to endogenous LepR activation^{22,38}, at lights-on after overnight feeding, when circulating
315 leptin levels are at their highest³⁹. While the number of P-STAT3-immunoreactive cells lying outside
316 the BBB in the vmARH was seen to be unaffected in *LepR*^{TankO} mice (Supplementary Figure 7A and
317 7B), the number of P-STAT-3 immunoreactive cells in the dmARH was diminished by about 30% in
318 these mutant mice when compared to *LepR*^{loxP/loxP} control littermates (Supplementary Figure 7A and
319 7C). We then assessed the ability of exogenous leptin to activate leptin-sensitive hypothalamic
320 neurons 15 min after an intraperitoneal (i.p.) bolus injection. While leptin-induced P-STAT3 activation
321 was unaffected in the vmARH (Figure 4A and 4B), it was still significantly hampered in the dmARH of
322 *LepR*^{TankO} mice when compared to *LepR*^{loxP/loxP} mice (Figure 4A and 4C). To determine how this
323 decreased access to peripheral leptin could impact the neuronal populations of the ARH involved in
324 the control of body homeostasis, we analyzed the expression of several key leptin-regulated
325 transcripts by q-PCR. Figure 4D shows that, in *LepR*^{TankO} mice, transcripts coding for the melanocortin
326 receptor antagonist *Agrp* were significantly induced, whereas *Socs3* mRNA levels were
327 downregulated. Next, we subjected *LepR*^{TankO} mice as well as their control littermates to an i.p. or
328 intracerebroventricular (i.c.v.) injection of exogenous leptin and measured food intake 24h (Figure 4E).
329 While exogenous leptin injected i.c.v. directly into the CSF was equally efficient in reducing feeding in
330 both groups of mice, *LepR*^{TankO} mice, in contrast to *LepR*^{loxP/loxP} mice, were unable to respond to
331 exogenous leptin injected i.p. by decreasing food intake (Figure 4E), suggesting once again that
332 tancytic LepR is necessary for peripheral leptin to reach leptin-sensitive neurons not in the immediate
333 vicinity of fenestrated vessels in the median eminence. Finally, we further verified that the decreased
334 response to peripheral leptin in *LepR*^{TankO} mice was due to an alteration in the LepR-dependent
335 tancytic transport of blood-borne leptin into the hypothalamus by implanting microdialysis probes into
336 the dorsomedial mediobasal hypothalamus of mutant mice and their control littermates (Figure 4F). In
337 agreement with the P-STAT3 distribution observed under physiological conditions (Supplementary
338 Figure 7), basal leptin levels in this region, before any dilution effect of peripheral vehicle injection,
339 were seen to be significantly lower in *LepR*^{TankO} mice (0.8±0.5 pg/ml) than in *LepR*^{loxP/loxP} littermates
340 (26.5±7.5 pg/ml, t-test, p=0.0196). In addition, 20 min after an i.p. bolus injection of leptin, *LepR*^{loxP/loxP}
341 mice displayed a significant early peak in hypothalamic leptin levels before reaching an intermediate
342 plateau and a second peak at 80 minutes, which were both absent in *LepR*^{TankO} mice (Figure 4F); in

343 the latter mice, leptin levels merely showed a small and non-significant rise at 60 min but remained at
344 near-nadir levels otherwise (Figure 4F).

345 Similarly, mice in which EGFR expression in tanycytes was blunted by the AAV1/2-mediated
346 expression of *Egfr* silencing RNAs in these cells (Supplementary Figure 4B, Figure 4G) phenocopied
347 certain aspects of *LepR*^{TanKO} mice, notably the concomitant decrease in lean mass and increase in fat
348 mass with no modification of body weight 8 weeks after infection, when compared with mice infected
349 with a control virus expressing GFP (Figure 4H, 4I and 4J). Like *LepR*^{TanKO} mice, animals with EGFR
350 silencing in tanycytes also showed a hampered ability to respond to an i.p. injection of leptin by
351 decreasing food intake (Figure 4K).

352 Altogether, these results strongly support the view that tanycytic LepR-EGFR signaling is required
353 for blood-borne leptin to be transported into the hypothalamus and exert its anorexigenic effect, and
354 reveals an unprecedented role for tanycytic leptin transport in the control of body composition.

355

356

357 **Mice lacking LepR in tanycytes show hyperlipidemia and lipid accumulation in white** 358 **adipocytes as well as in the liver**

359 Given the increase in RER in *LepR*^{TanKO} mice (Figure 3M), indicative of the increased consumption
360 of carbohydrates over lipids to meet energy requirements⁴⁰, we next examined how lipid metabolism
361 was altered in mice in which leptin transport into the hypothalamus was defective. The changes in
362 RER and food-intake-independent body weight gain in *LepR*^{TanKO} mice appeared to be due to
363 decreased fatty acid oxidation (Figure 5A), which was associated with an increase in both visceral fat
364 mass (Figure 3I) and leptinemia (Figure 3O) and elevated circulating levels of cholesterol and
365 triglycerides (Figure 5B), but not of non-esterified free fatty acids (NEFAS) (Figure 5C). These data,
366 together with an increase in the size of white adipocytes (Figure 5D), suggest that *LepR*^{TanKO} mice
367 show hyperlipidemia and lipid accumulation in white adipocytes.

368 In agreement with the increased uptake of free fatty acids into white adipose tissue in response to
369 central leptin deficiency¹³, *LepR*^{TanKO} mice showed a marked increase in protein levels of lipoprotein
370 lipase (LPL), an enzyme that promotes the uptake of circulating triglycerides, and acetyl-CoA
371 carboxylase (Acc) and fatty acid synthase (FAS), enzymes crucial for *de novo* lipogenesis, in
372 ependymal fat (Figure 5E and 5F). Of note, the ratio of phospho-Acc to total Acc was decreased in

373 *LepR*^{Tan^{KO}} mice (Figure 5E and 5F), which suggests, in agreement with previously published data ¹³,
374 that hypothalamic leptin regulates ACC in white adipose tissue. We next examined the expression of
375 the key lipolytic enzyme hormone-sensitive lipase (HSL), the activity of which is also known to be
376 regulated by central leptin signaling ¹³, and found that the levels of phosphorylation-activated HSL
377 were lower in *LepR*^{Tan^{KO}} mice than in control littermates (Figure 5E and 5F). Overall, these results
378 indicate that the lack of LepR in tanycytes favors the accumulation of lipids by promoting lipogenesis
379 and lipid uptake while inhibiting lipolysis in white adipose tissue. Importantly, these effects were
380 independent of feeding since they occurred in both *LepR*^{Tan^{KO}} mice fed *ad libitum* and those pair-fed
381 with the control group.

382 Increased accumulation of lipids was also noted in the liver of *LepR*^{Tan^{KO}} mice using oil red staining
383 (Figure 5G). Accordingly, liver triglyceride content was seen to be increased in these mice even in the
384 pair-fed condition (Figure 5H), whereas circulating triglyceride levels were comparable to those in
385 *LepR*^{loxP/loxP} controls (Figure 5B). Given the absence of any marked change in the expression of
386 enzymes involved in lipid metabolism (Figure 5I and 5J), the increase in lipid accumulation in the liver
387 of *LepR*^{Tan^{KO}} mice is likely not due to local *de novo* synthesis but indirectly to the increased weight and
388 hyperlipidemia of these mice.

389

390 **Mice lacking LepR in tanycytes sequentially develop impaired glucose tolerance and defective** 391 **insulin-secretory capacity**

392 Leptin has long been known to influence glucose homeostasis independent of its effect on body
393 weight regulation ^{41,42}. These effects appear to be mediated by leptin action on LepR-expressing
394 neurons in the ARH, since the local reintroduction of LepR expression in otherwise LepR-knockout
395 animals normalizes insulinemia in these animals ¹¹. In light of the altered gene expression in ARH
396 neurons observed in our mice, we therefore next investigated the effect of LepR deletion in tanycytes
397 in glucose metabolism. Four weeks after LepR deletion, mice did not appear to have any problem in
398 managing exogenous injections of glucose (Figure 6A). However, monitoring glucose-stimulated
399 insulin release in *LepR*^{Tan^{KO}} mice at 4 weeks intriguingly showed that, despite normal glucose
400 tolerance at this early time point (Figure 6A), these mice were secreting more insulin than control
401 *LepR*^{loxP/loxP} or *LepR*^{Tan^{Het}} mice both before (12h fasting insulin: *LepR*^{Tan^{KO}}, $0.81 \pm 0.12 \mu\text{g}/\mu\text{l}$ vs.
402 *LepR*^{loxP/loxP}, $0.48 \pm 0.06 \mu\text{g}/\mu\text{l}$ and *LepR*^{Tan^{Het}}, $0.46 \pm 0.03 \mu\text{g}/\mu\text{l}$, $p = 0.03$ and $p = 0.04$, respectively,

403 one way ANOVA and Tukey's multiple comparison test) and after glucose injection (Figure 6B),
404 despite an apparently normal response to insulin (Figure 6C), suggestive of a pancreatic β -cell
405 function deficiency. This elevated release of insulin by β -cells even under basal conditions
406 phenocopies mice lacking LepR in POMC neurons⁴³, concordant with an inability of ARH neurons to
407 appropriately perceive circulating leptin levels as suggested by decreased STAT3 activation after
408 overnight feeding (Supplementary Figure 7) or upon exogenous leptin treatment (Figure 4A, 4C), as
409 well as the downregulation of *Socs3* in the ARH of *LepR*^{TankO} mutants (Figure 4D).

410 By 12 weeks after LepR deletion, however, *LepR*^{TankO} mice developed impaired tolerance to
411 exogenous glucose (Figure 6D), while their basal insulin levels were similar to those in *LepR*^{loxP/loxP}
412 mice. This deficient glucose homeostasis was also correlated with a significantly lower increase in
413 glucose-stimulated insulin levels in *LepR*^{TankO} mice, suggesting some degree of pancreatic dysfunction
414 in these mice (Figure 6E). Insulin sensitivity and HOMA-IR were similar in the two genotypes (Figure
415 6F and 6G). To investigate possible alterations in pancreatic function in mice lacking LepR in
416 tanycytes, we investigated glucose-stimulated insulin secretion (GSIS) in isolated pancreatic islets
417 from *LepR*^{TankO} and *LepR*^{loxP/loxP} littermates. Although *LepR* deletion in tanycytes did not affect the total
418 insulin content of islets (Figure 6H), insulin secretion from isolated islets was severely hampered
419 under high glucose conditions in 12-week *LepR*^{TankO} mice when compared to *LepR*^{loxP/loxP} controls
420 (Figure 6I). Gene expression analysis in islets from 12-week *LepR*^{TankO} mice compared to controls
421 revealed the increased expression of genes involved in glucose sensing (*Glut2*, *Gck*) and insulin
422 maturation (*Pcsk1*) but decreased expression of key β -cell identity genes such as *Pdx1* ($p=0.065$) and
423 *MafA* (Figure 6J). *LepR*^{TankO} islets also exhibited an increase in the expression of markers of the
424 endoplasmic reticulum (ER) unfolded protein response (UPR^{er}) pathway, including *Atf4* ($p=0.016$),
425 *Xpb1t* and *Chop* (Figure 6K), thought to be associated with impaired β -cell function and T2D
426 development⁴⁴. The number of α (glucagon-positive) and β (insulin-positive) cells per islet was similar
427 in the pancreas of the two genotypes (Figure 6L, 6M, 6N). Altogether, these data suggest that the loss
428 of *LepR* function in tanycytes impairs glucose homeostasis and insulin secretion through the
429 transcriptional control of key pancreatic β -cell and UPR^{er} markers, preceded by the development of
430 mild insulin resistance, and that the whole sequence of events unfolds within 3 months of altering the
431 tanycytic shuttling of leptin into the hypothalamus.

432 To determine whether the restoration of hypothalamic access to leptin could rescue β -cell function in
433 12-week $LepR^{TanKO}$ mice, we deprived animals of food 3h before stereotaxically injecting them with 2
434 μ g of leptin i.c.v., shortly before lights-off. At lights-on, i.e. 12h after leptin injection in food-deprived
435 animals, a glucose tolerance test was performed by injecting glucose i.p. Pre-treatment with acute
436 i.c.v. leptin significantly rescued the impaired glucose management in $LepR^{TanKO}$ mice, without further
437 depressing glycemia in $LepR^{loxP/loxP}$ littermates (Figure 6O). In addition, while glucose-stimulated
438 insulin secretion at 15 min was lower in mice lacking tanycytic LepR than in $LepR^{loxP/loxP}$ littermates in
439 the absence of leptin pre-treatment, as shown above (Figure 6E), the central administration of leptin
440 significantly increased insulin secretion 15 min after glucose injection in both mutant and control mice,
441 compensating for the defective tanycytic function (Figure 6P). These results demonstrate that the
442 action of tanycyte-transported leptin in the hypothalamus is vital for the acute control of β -cell function
443 directly by the brain, likely through the intermediary of leptin-sensing ARH neurons connected to the
444 pancreas via the autonomic nervous system⁴³, and raise the intriguing possibility that defects in the
445 tanycytic leptin shuttle may also play a critical central role in the pathophysiology of diabetes.

446

447 **Impaired access of leptin to the hypothalamus could mediate central effects on glucose and** 448 **lipid metabolism through altered sympathetic tone**

449 The central effects of leptin on glucose homeostasis appear to involve the melanocortin system⁴³,
450 which we have shown above to be altered in $LepR^{TanKO}$ mice, and which impinges upon the
451 sympathetic nervous system^{45,46}. In addition, the sympathetic nervous system is also known to
452 mediate the central effects of leptin on white adipose tissue lipid metabolism¹³. We therefore next
453 assessed circulating noradrenaline levels in $LepR^{TanKO}$ mice, with their defective tanycytic shuttling of
454 leptin into the hypothalamus (Figure 4E and 4F), and found that the levels of noradrenaline were
455 reduced, suggesting an overt decrease in sympathetic tone when compared to control $LepR^{loxP/loxP}$
456 littermates (Figure 7A). Interestingly, the pancreatic islets of $LepR^{TanKO}$ animals express more α 2A
457 adrenergic receptors compared to their littermates without affecting the expression of β 2 adrenergic
458 receptors (Figure 7B). α 2A adrenergic receptors are known for their inhibitory action on insulin
459 secretion by the pancreas^{47,48}. To further probe the sympathetic nervous system in $LepR^{TanKO}$ mice,
460 we subjected them to a 2h exposure to cold (4°C) and measured changes in rectal temperature as
461 well as noradrenaline levels. In cold conditions, $LepR^{TanKO}$ mice experienced a drop in core

462 temperature (Figure 7C), a phenomenon associated with defective cold-induced noradrenaline
463 secretion (Figure 7D). Together, these results suggest a possible mechanistic pathway whereby
464 decreased leptin access to hypothalamic neurons controlling bodily homeostasis alters overall
465 sympathetic tone, which in turn affects peripheral glucose and lipid metabolism. Because previous
466 studies have shown that brain-pancreas and brain-adipose tissue connections involve leptin signaling
467 through the melanocortin system^{43,49} and because *LepR*^{TankO} mice show altered levels of *Agrp*
468 transcripts (Figure 4D), it is tempting to speculate that the main hypothalamic neuronal population
469 affected by the defective shuttling of circulating leptin into the brain is that of AgRP-expressing ARH
470 neurons, which mediate melanocortin signaling.

471

472 **Knocking out LepR in tanycytes blunts the leptin-mediated neuroendocrine response to fasting**

473 Given our previous demonstration that tanycytes play a role in the adaptive response to fasting²², and
474 because leptin has long been known to play important physiological roles during starvation⁵⁰, we next
475 tested the ability of peripheral leptin treatment (1mg/kg/12h) to attenuate the adaptive neuroendocrine
476 response to 24h fasting in *LepR*^{TankO} mice. While leptin repletion after this period of starvation had no
477 effect on blood glucose, it caused a reduction in food intake over the first 4h and 12h of refeeding and
478 a consequent reduction in weight gain after 24h in *LepR*^{loxP/loxP} mice, but not in *LepR*^{TankO} littermates
479 (Figure 7E). Interestingly, while 24h fasting dramatically increased corticosterone levels in *LepR*^{loxP/loxP}
480 mice, a phenomenon normalized by leptin replacement therapy, it did not cause any change in
481 corticosterone levels in *LepR*^{TankO} mice (Figure 7E).

482 Overall, our results strongly suggest that in the absence of the tanycytic leptin shuttle, the brain loses
483 its ability to properly respond to physiological challenges and thus to restore bodily homeostasis.

484

485

486 **DISCUSSION**

487

488 Leptin, a hormone secreted by adipocytes in the periphery, plays a fundamental role in the regulation
489 of energy homeostasis by controlling food intake and energy expenditure⁴⁻⁹. To achieve its central
490 effects, leptin needs to cross the blood-brain barrier and gain access to specific leptin-sensitive
491 neurons in the hypothalamus and elsewhere, a process mediated by tanycytes²³. Our results
492 convincingly show that, in contrast to recent studies that question the expression of the leptin receptor
493 *LepR* in tanycytes²⁵, *LepR* is not only expressed but is functionally active in hypothalamic median

494 eminence tanycytes, and transports leptin into the hypothalamus in a leptin- and EGF-dependent
495 manner by forming a complex with EGFR.

496 Possible explanations for the assumption that LepR is not expressed in tanycytes could be the fact
497 that, like astrocytes, these specialized hypothalamic glia do not express the cre-dependent reporter
498 genes commonly used in *LepR::Cre* animal models²⁴ or that most of the alternative detection
499 techniques used so far are not sensitive enough²⁵. In addition, in the inducible Cre-driver mouse lines
500 used by others²⁵, the accessibility of the *LepR* gene in tanycytes may be impaired by the use of
501 tamoxifen, which is known to alter chromatin architecture⁵¹, interfere with estrogen receptor activity
502 and impact metabolism on its own⁵². These technical problems were overcome in the current study
503 with an array of methods to detect not only the presence of LepR protein in ME tanycytes but also its
504 function. In addition, we demonstrate that LepR signaling in tanycytes plays a critical role in the
505 transcytotic mechanism by which they shuttle blood-borne leptin into the hypothalamus, and show that
506 the leptin-mediated activation of LepR causes the early activation of EGFR, which we had previously
507 and serendipitously shown to be able to rescue diet-induced obese animals from central resistance to
508 peripheral leptin²³. This leptin-LepR-dependent activation of EGFR in tanycytes, which our PLA
509 experiments suggest occurs in tanycytic distal processes that contact the fenestrated endothelium of
510 pituitary portal capillaries *in vivo*, is required for the release of internalized leptin from early
511 endosomes by triggering the downstream ERK signaling pathway. Furthermore, while LepR and
512 EGFR appear to form a complex capable of binding both leptin and EGF, the activation of EGFR by
513 EGF potentiates the effects of leptin on ERK activation while it appears to leave P-STAT3 activation
514 unaffected. The kinetics of EGFR and ERK activation by leptin in primary tanycytes, with the leptin-
515 induced phosphorylation of EGFR occurring at very early time points, within 2 minutes as seen by
516 PamGene technology, and ERK phosphorylation occurring at 15 min, is reminiscent of that reported in
517 gastric cancer cells⁵³. Although we detected EGF in the circulation in our animals, this EGFR
518 activation in tanycytes could also involve *trans*-activation processes, similar to those observed in
519 cancer cells⁵³ and also known to occur in tanycytes^{54,55}.

520 Leptin signaling in the brain also exerts specific and complementary peripheral effects on adipose
521 tissue through the regulation of nutrient partitioning by decreasing the expression of key *de novo*
522 lipogenic enzymes and stimulating the levels of phosphorylated HSL, essential for the activation of
523 lipolysis^{7,13}. Interestingly, in addition to its mild consequences on body weight, we show that deleting

524 tancytic LepR expression in the median eminence of adult mice increases food intake, modifies
525 nutrient partitioning to favor the disproportionate use of carbohydrates, thus favoring lipid
526 accumulation, dramatically alters body composition by promoting an increase in fat mass to the
527 detriment of lean mass, and also impairs the ability of the brain to control glucose homeostasis in
528 association with a marked impairment in pancreatic β -cell function and altered sympathetic tone.

529 The capacity of leptin to regulate these diverse metabolic parameters resides in LepR-expressing
530 neurons in the ARH, namely proopiomelanocortin (POMC) and agouti-related peptide (AgRP)
531 expressing neurons, which are known to be involved in the control of adipose tissue lipogenesis¹³ and
532 glucose homeostasis¹¹, in response to this adiposity signal. For instance, the deletion of LepR in
533 either POMC or AgRP neurons leads to moderate obesity, while the knock-out of LepR in both AgRP
534 and POMC neurons combined has clear cumulative effects on adiposity despite a comparable effect
535 on food intake^{56,57}. The fact that our mice mimic this metabolic phenotype suggests that the depletion
536 of LepR in tancytes precludes the access of leptin to POMC and AgRP neurons and its subsequent
537 actions in these neuronal populations. This hypothesis is supported by the fact that the removal of
538 LepR from tancytes severely hampers the ability of both endogenous and exogenous leptin to reach
539 the mediobasal hypothalamus and activate leptin-sensitive neurons in the dmARH, and upregulates
540 transcripts for *Agrp*, a melanocortin receptor antagonist, while downregulating the expression of
541 *Socs3*, a known leptin-responsive gene³⁶, in the ARH. Interestingly, the melanocortin system is
542 involved not only in glucose homeostasis^{11,43,58} but also in the sympathetic nervous system-mediated
543 regulation of lipid metabolism in white adipose tissue^{13,49}, and both nadir and cold-induced circulating
544 noradrenaline levels are reduced in mice lacking tancytic LepR. In light of these findings, we propose
545 that deficient leptin-regulated activity in POMC and AgRP neurons of the dmARH alters their capacity
546 to use the melanocortin signaling pathway^{59,60} to communicate with neurons of the autonomous
547 nervous system in the brainstem and the spinal cord^{45,61}, and thus their control of peripheral target
548 tissues^{7,62}. In keeping with the hypothesis above, we found that the decrease in insulin secretion by
549 pancreatic β -cells in mice lacking LepR in tancytes was associated with a significant increase in their
550 expression of α 2A adrenergic receptors. This is also in agreement with previous studies showing that
551 the activation of these receptors is associated with a decrease in both glucose tolerance and insulin
552 exocytosis by β islets⁴⁷. In addition, in humans, a polymorphism leading to the overexpression of the
553 α 2A adrenergic receptor ADRA2A is associated with an increased risk of developing T2D⁴⁸. Our

554 results suggest that the removal of leptin receptor expression in tanycytes may lead to a decrease in
555 insulin secretion that can be explained by an overexpression of adrenergic receptors $\alpha 2A$. Overall, our
556 results fill the gaps in our understanding of the mechanism of leptin action: i) blood-borne leptin
557 reaches dmARH neurons through a singular route involving transcytotic transport by median eminence
558 tanycytes, which depends on the activation of a LepR:EGFR complex and ERK signaling, ii) leptin
559 then stimulates the dmARH neurons controlling the melanocortin system and sympathetic outflow, and
560 iii) this diminishes lipid storage in adipose tissue and controls glucose homeostasis by shaping the
561 function and plasticity of pancreatic islet cells through their expression of $\alpha 2A$ adrenergic receptors..
562 Conversely, alterations in tanycytic leptin transport manifest as decreased sympathetic tone,
563 increased visceral adiposity, hepatic steatosis and glucose intolerance with pancreatic dysfunction.
564 Interestingly, regardless of whether LepR or EGFR signaling in tanycytes is defective in our mouse
565 models, the fat mass gain observed occurs concomitantly with an intriguing loss of lean tissue,
566 resulting in overall weight gain remaining limited. This phenomenon, where obesity is associated with
567 sarcopenia (sarcobesity), is reminiscent of that often seen during aging^{63,64} and may promote the
568 progression of related conditions such as diabetes and frailty⁶⁵. A recent study has shown that in
569 mouse models of hyperglycemia and T2D due to defective β cell function, inter-tissue crosstalk
570 involving the liver and amino acid catabolism leads to skeletal muscle atrophy⁶⁶. Further studies are
571 required to explore this pathway in mice in which LepR:EGFR signaling complex is defective in
572 tanycytes, to determine how alterations of the tanycytic leptin shuttle impact aging.

573 Longitudinal human studies show that T2D develops in subjects exhibiting insulin hypersecretion in
574 normoglycemic and prediabetic phases in order to keep glycemia near normal, in a context of chronic
575 nutrient surfeit and obesity-associated insulin resistance, until they reach a threshold at which this
576 compensatory β cell response becomes unsustainable⁶⁷. Compensating for insulin resistance by
577 increasing insulin secretion usually requires both enhanced β cell function and expansion of the β cell
578 mass, the latter being stimulated by the increased nutrient supply, including glucose and free fatty
579 acids⁶⁸. However, diabetes is a heterogeneous disease⁶⁹, and an alternative pattern characterized by
580 the alteration of insulin secretion due to a β cell functional deficit could predominate in some ethnic
581 groups. This phenotypic variability can be seen in a Japanese study in which the proportion of patients
582 progressing to the onset of T2D was 50% in patients with a dysfunction of isolated β cells, as
583 compared to 14% for patients with insulin resistance⁷⁰. Intriguingly, an epidemiological study of

584 Korean patients with T2D showed that they developed impaired insulin secretion and insulin
585 resistance 10 years before the onset of diabetes, and impaired β cell compensation with an abrupt
586 decrease in insulin secretion during the last 2 years before onset ³, underscoring the central role of β
587 cell dysfunction in the pathogenesis of T2D in Asian populations. The existence of two patterns of
588 disease progression can also be seen from the fact that East Asian T2D patients have a much lower
589 BMI than European patients but more intra-abdominal fat for similar BMI values ². In our current
590 model, the attenuation of tanycytic leptin transport leads to an initial increase of insulin secretion
591 despite the absence of insulin resistance. Twelve weeks after selectively deleting LepR in median
592 eminence tanycytes, *LepR*^{TanKO} mice develop impaired insulin secretion in response to glucose,
593 against a backdrop of increased visceral fat but normal insulin sensitivity. This alteration of glucose-
594 stimulated insulin secretion, which likely underlies the alteration of glucose homeostasis, can be seen
595 at the level of isolated pancreatic islets despite the lack of any apparent change in their size or
596 organization, suggesting a modification of β cell functional integrity instead, mimicking the principal
597 human phenotype described above. Despite this deficiency in β -cell function, the reactivation of
598 central control by infusing leptin into the cerebral ventricles 12 weeks after the tanycytic leptin shuttle
599 was inactivated by knocking out LepR restored the ability of these mice to manage exogenous
600 glucose, by restoring insulin secretion induced by CSF-borne leptin.

601 To summarize, the study of our *LepR*^{TanKO} mouse model appears to have unmasked two important
602 aspects of leptin action: i) the molecular and cellular mechanisms that regulate the physiological
603 access of leptin to leptin-responsive neurons in the brain, i.e. the LepR-EGFR-ERK-mediated
604 transcytotic transport of blood-borne leptin into the hypothalamus by tanycytes, and ii) the link
605 between deficient leptin transport by tanycytes and the pathophysiology of pancreatic β -cell failure and
606 lipid dysmetabolism in the context of moderate overweight and sarcobesity. Together, these findings
607 shed light on the central control of peripheral lipid and glucose homeostasis by leptin, and create new
608 therapeutic avenues for metabolic disorders.

609

610 **METHODS**

611 **Animals**

612 All C57Bl/6J mice were housed under specific pathogen-free conditions in a temperature-controlled
613 room (21-22°C) with a 12h light/dark cycle and *ad libitum* access to food and water. *tdTomato*^{loxP-STOP-}

614 ^{loxP} (IMSR Cat# JAX:007914, RRID:IMSR_JAX:007914) and GCamP3^{loxP-STOP-loxP} (IMSR Cat#
615 JAX:025406, RRID:IMSR_JAX:025406) reporter mice and *LepR*^{loxP/loxP} mice (IMSR Cat# JAX:008327,
616 RRID:IMSR_JAX:008327)⁷¹ were purchased from the Jackson Laboratories (Bar Harbor, ME).
617 *Trmp5::Cre* mice have been engineered by Dr. Ulrich Boehm (University of Saarland, Homburg,
618 Germany) and published elsewhere²⁹. Animal studies were approved by The Institutional Ethics
619 Committees for the Care and Use of Experimental Animals of the University of Lille; all experiments
620 were performed in accordance with the guidelines for animal use specified by the European Union
621 Council Directive of September 22, 2010 (2010/63/EU).

622

623 **TAT-Cre, pAAV-Dio2-iCre-2A-GFP and AAV(1+2)-GFP-U6-m-EGFR-shRNA delivery**

624 A TAT-Cre fusion protein and the AAV 1/2 *Dio2::Cre* virus (0,5x10¹⁰ genomic particles per μ l) were
625 produced as detailed previously^{31,72}. AAV(1+2)-GFP-U6-m-EGFR-shRNA was produced by Vector
626 Biolabs (shAAV-258137). All products were stereotaxically infused into the third ventricle (2 μ L over 7
627 min at 1,27 mg/ml; anteroposterior, -1.7 mm; midline, 0 mm; dorsoventral, -5.6 mm), the lateral
628 ventricle (Anteroposterior, -0.3 mm; midline, +/- 1 mm; dorsoventral, -3 mm) or the fourth ventricle
629 (Anteroposterior, -6 mm; midline, 0 mm; dorsoventral, -4 mm) of 24h fasting isoflurane-anesthetized
630 floxed mice 1 week before experiments for the TAT-Cre one and 3 weeks before experiments for the
631 virus one.

632

633 ***Evaluation of TAT-Cre recombination efficiency***

634 Four weeks after lateral ventricle or 3rd ventricle TAT-Cre infusion in *TdTomato* mice, animals were
635 anesthetized with ketamine (8mg/kg body weight) + xylazine (3mg/kg body weight) before being
636 perfused with Saline (0,9% NaCl) and 4% paraformaldehyde. Brains were collected before being
637 cryoprotected in 20% sucrose solution overnight, embedded in Tissue Tek (Sakura®) and frozen
638 freshly. 16 μ m-thick coronal sections were cut and processed for immunofluorescence using chicken
639 anti-Vimentin (1:2000; Millipore Cat# AB5733, RRID:AB_11212377) primary antibodies and Alexa647-
640 conjugated anti-chicken antibody (1/1000; Thermo Fisher Scientific Cat# A-21449,
641 RRID:AB_2535866). Images were acquired using an Axio Imager Z2 Apotome microscope (AxioCam
642 MRm camera, Zeiss). 8 median eminence representative slides per animal were then coded to
643 conceal treatment groups and the tanycytes (Vimentin positive cells) were divided into three groups

644 depending their projections (median eminence and arcuate nucleus, ventromedial hypothalamus,
645 dorsomedial hypothalamus). Number of DAPI+/Tomato+/Vimentin+ cells was reported on
646 DAPI+/Vimentin+ cells bordering the 3rd ventricle. The ratio was compared between different groups.
647 To compare 3rd and 4th ventricle TAT-Cre infusion, the number of FACS -sorted Tomato positive cells
648 was compared in ME and 4th ventricle microdissected samples, 1 week after TAT-cre infusion.

649

650 **Fluorescence-Activated Cell Sorting and Real-Time PCR Analyses**

651 ***Isolation of hypothalamic tanycytes using Fluorescence Activated Cell Sorting***

652 Median eminence from TAT-Cre injected *tdTomato*^{loxP/+} and *LepR*^{oxP/loxP}; *tdTomato*^{loxP/+} mice were
653 microdissected, and enzymatically dissociated using Papain Dissociation System (Worthington,
654 Lakewood, NJ) to obtain single-cell suspensions. FACS was performed using an ARIA SORP cell
655 sorter cytometer device (BD Bioscience, Inc). The sort decision was based on measurements of
656 tdTomato fluorescence (excitation 561nm; detection: bandpass 675+/-20nm) by comparing cell
657 suspensions from tdTomato positive and wild-type animals, as indicated in Figure 3A. For each
658 animal, 4000 cells tdTomato positive and negative cells and negative cells were sorted directly into
659 10µL extraction buffer: 0,1% Triton® X-100 (Sigma-Aldrich) and 0,4 U/µl RNaseOUT™
660 (ThermoFisher).

661

662 ***Quantitative RT-PCR analyses***

663 For gene expression analyses, mRNAs obtained from microdissected hypothalamic explants or FACS-
664 sorted tanycytes were reverse transcribed using SuperScript® III Reverse Transcriptase (Life
665 Technologies) and a linear preamplification step was performed for the sorted cells only using the
666 TaqMan® PreAmp Master Mix Kit protocol (P/N 4366128, Applied Biosystems). Real-time PCR was
667 carried out on Applied Biosystems 7900HT Fast Real-Time PCR System using exon-boundary-
668 specific TaqMan® Gene Expression Assays (Applied Biosystems): DARPP32
669 (*Ppp1r1b*_Mm00454892_m1); LEPR (Variant 1, long form) (*LepR*_Mm1265583_m1); LEPR (Variant
670 3, short form) (*LepR*_Mm01262070_m1), NPY (*NPY*-Mm03048253_m1), MECA32 (*Pivap*-
671 *Mm00453379_m1*), POMC (*POMC*-Mm00435874_m1), AgRP (*AgRP*-Mm00475829_g1), CART
672 (*CARTPT*-Mm04210469_m1), *Socs3* (*Socs3*-Mm00545913_s1), *Ptp1b* (*Ptp1b*-Mm00448427_m1)
673 *DIO2* (*Dio2*-Mm00515664_m1), *FGF10* (*Fgf10*-Mm00433275_m1), *GPR50* (*Gpr50*-

674 Mm00439147_m1), SLCO1C1 (Slco1c1-Mm00451845_m1). Control housekeeping genes: r18S (18S-
675 Hs99999901_s1); ACTB (Actb-Mm00607939_s1). Gene expression data were analyzed using SDS
676 2.4.1 and Data Assist 3.0.1 software (Applied Biosystem).

677 **Physiological measurements**

678 ***Body Composition***

679 Body composition was measured weekly in several cohorts of mice using Minispec LF Series (Bruker
680 Corporation, Massachusetts). Data on fat mass, lean mass and free liquid mass were collected and
681 expressed as % of body weight.

682 ***Analysis of basal metabolism***

683 Mice were analyzed for total energy expenditure, oxygen consumption and carbon dioxide production,
684 food intake and ambulatory movements (total beam breaks/h) using calorimetric cages (TSE Systems
685 GmbH, Germany) and standard procedures. Mice were individually housed and acclimatized to the
686 cages for 48h before experimental measurements. During the pair-fed test, paired-fed animals had the
687 mean weight of food that the control group ate during the previous 24 hours (see paragraph below).
688 RER and energy expenditure (EE) were calculated as previously reported by us ^{73,74}, and fatty acid
689 oxidation was calculated using the formula reported by Bruss and colleagues ⁷⁵:

$$690 \qquad \qquad \qquad \text{FA oxidation (kcal/h)} = \text{EE} \times (1 - \text{RER}/0.3)$$

691 ***Pair-feeding experiments***

692 Pair-feeding experiments were performed as documented previously ^{76,77}. Briefly, we assessed food
693 intake under normal conditions in both LepR^{loxP/loxP} and LepR^{TanKO} mice for at least one week without
694 performing any type of experiment and avoiding any stress. Then, we pair-fed LepR^{TanKO} mice with the
695 group showing lower food intake, i.e., LepR^{loxP/loxP} mice. To avoid long periods of fasting that could
696 alter the results obtained from the pair-fed group, pair-fed LepR^{TanKO} mice received 2/3 of their
697 daily amount of food just before the dark phase (the active period when mice consume the highest
698 amounts of food) and 1/3 at lights-on (the period when mice are inactive and consume low amounts of
699 food).

700

701 ***Glucose Tolerance Test and Insulin dosage***

702 Mice were fasted overnight before the experiment (12 hours). Blood sample for insulin dosage was
703 taken before, 15 and 30 min after glucose administration with glass capillary at the tail. Samples were
704 kept on ice during the experiments before being centrifuged (4°C, 600 rpm, 15 min) to collect serum
705 and frozen at -80°C until insulin ELISA (Mercodia). Basal blood glucose level was measured before
706 glucose i.p administration (1,5 mg glucose/g of body weight), 15, 30, 45, 60, 120 and 150 min after
707 glucose administration using glucometer (OneTouch® Verio meter). One cohort of animals was
708 injected i.c.v with recombinant murine leptin (2µg/animal; Harbor-UCLA Medical Center, California) 3
709 hours before lights-off, mice subjected to fasting overnight (12 hours) and glucose tolerance test as
710 well as insulin dosage performed the next day.

711 ***Insulin Tolerance Test***

712 Mice were fasted 6 hours before the experiment. Basal blood glucose level was measured before
713 insulin i.p administration (0,75UI/kg of body weight), 15, 30, 45, 60, 120 and 150 min after glucose
714 administration using glucometer (OneTouch® Verio meter)

715 ***In vivo leptin sensitivity test***

716 Mice were first separated one per cage and fasted during 3 hours in the afternoon. Then they are
717 divided into two groups which received i.p or i.c.v injections of recombinant murine leptin (3mg/kg;
718 Harbor-UCLA Medical Center, California) or vehicle (PBS pH 8.0) 3 hours before being refeed. Body
719 weight and food intake were measured before, 12h and 24h after treatment period.

720 ***Assessment of the role of leptin in the corticosterone response to 24h fasting***

721 Two weeks before fasting, at lights-on (8 am), glycemia was measured and blood was drawn from the
722 animal's cheek ⁷⁸ to assess serum corticosterone levels in the fed condition. Then, mice were put in
723 individual cages and subjected to fasting for 24 hours. Half the fasting mice received leptin (1mg/kg;
724 Harbor-UCLA Medical Center, California) while the other half received saline i.p. injections every 12
725 hours (8 am and 8 pm). After 24h of fasting, blood samples were taken from each animal's cheek
726 before refeeding. Food intake was then measured at 4, 12 and 24 hours after refeeding.

727 Corticosterone levels were quantified by ELISA (55-CORMS-E01; American Laboratory Products
728 Company) according to manufacturer's instructions.

729 **Cold-exposure test: core temperature and noradrenaline measurements**

730 Rectal temperature was measured in mice before collecting blood samples from the cheek. One hour
731 later, mice were exposed to cold (4°C) for 2 hours, then rectal temperature was taken and blood
732 collected. Delta temperature (difference between before and after cold exposure) was calculated and
733 fed and fasting noradrenaline serum concentrations were quantified by ELISA (see paragraph below).

734 **Microdialysis *in vivo***

735 Nine *LepR^{loxP/loxP};tdTomato^{loxP-STOP-loxP}* mice were injected in the lateral ventricle with the AAV(1/2)
736 *Dio2::Cre* virus (n=4) or vehicle (n=5). In brief, 25-35g mice were deeply anesthetized with isoflurane
737 (3% in 1 L/min air flow) in an induction chamber, placed in a stereotaxic apparatus equipped with a
738 mask to maintain anesthesia during all the experiment (isoflurane between 1 to 1.5% in 1 L/min air
739 flow). Core body temperature was maintained at 37°C with an electrical blanket controlled by a
740 thermostat. A microdialysis cannula (CMA8 High Cut-off, 100 kDa, 1 mm membrane length; CMA
741 microdialysis AB, Sweden) was implanted over the mediobasal hypothalamus using the stereotaxic
742 coordinates (relative to bregma antero-posterior: -1.3, lateral: -0.3, ventral from brain: -6.1 mm). The
743 microdialysis probe was then perfused with sterile artificial cerebrospinal fluid (CMA Perfusion Fluid
744 CNS. NaCl 147 mmol/L, KCl 2.7mmol/L, CaCl₂, 1.2 mmol/L and MgCl₂ 0.85 mmol/L; CMA,
745 Stockholm, Sweden) at a rate of 2 µL/min using a microinjection pump (CMA 402; CMA, Stockholm,
746 Sweden). Following a stabilization period of 45 min, one dialysate of 20 min was collected as basal. A
747 vehicle injection (i.p, PBS pH 8.0) was administered to the mice and two dialysates of 20 min were
748 recovered. Finally, at 60 min, a leptin solution was administered to the mice (i.p, 3mg/Kg in PBS pH
749 8.0, Harbor-UCLA Medical Center, California) and 5 dialysates of 20 min each were recovered. Brain
750 dialysates were placed in a fraction collector (CMA/820) during the experiment and immediately stored
751 at -80°C until analysis. At the end of the experiment, mice were euthanized by decapitation and brains
752 stored immediately in fresh paraformaldehyde 4%. Vibratome brain sections of 80 µm were
753 counterstained with DAPI to verify probe location. Only mice in which the probe was positioned
754 between antero-posterior: -1.2 and -2.3 were included in the analysis.

755 ***Leptin, EGF and noradrenaline ELISA assays***

756 Basal leptin concentration in the serum of *LepR^{loxP/loxP}* and *LepR^{TankO}* mice and leptin content in
757 microdialysates from the brain were measured using ELISA (Leptin mice MOB00; R&D systems)
758 according to the manufacturer's protocol. EGF concentration in blood serum from C57Bl/6J mice fed
759 normal chow or 8 weeks of high-fat diet (#D12492; Research Diets), *LepR^{loxP/loxP}* and *LepR^{TankO}* mice
760 were quantified by ELISA according to the manufacturer's instructions using a mouse EGF ELISA kit
761 (EMEGF ; ThermoFisher). Basal noradrenaline concentrations in the serum of *LepR^{loxP/loxP}* and
762 *LepR^{TankO}* mice were quantified using a noradrenaline ELISA kit (BA-E5200; Immusmol).

763 **Brain and peripheral tissues analysis**

764 ***Brain slice preparation and calcium imaging***

765 Eight to 12 week-old male *GCaMP3^{Trmp5}* and *GCaMP3^{Trmp5}*; *LepR^{Trmp5}* mice were anesthetized with
766 isoflurane, and after decapitation, the brain was rapidly removed and put in ice-cold oxygenated (O₂
767 95% / CO₂ 5%) artificial cerebrospinal fluid (ACSF) containing the following (in mM): 120 NaCl, 3.2
768 KCl, 1 NaH₂PO₄, 26 NaHCO₃, 1 MgCl₂, 2 CaCl₂, 10 glucose (300 mOsm, pH 7.4). After removal of the
769 cerebellum, the brain was glued and coronal hypothalamic slices 200 μm thick containing the median
770 eminence and lateral walls of the third ventricle were cut using a vibratome (VT1200S; Leica) as
771 previously described⁷⁹. Before recording, slices were incubated at 35°C for a recovery period of 1 h.
772 After recovery, slices were placed in a submerged recording chamber (31°C; Warner Instruments) and
773 continuously perfused (2 ml/min) with oxygenated ACSF. Tanycytes were observed with a 40x water
774 immersion objective in an upright Leica DM-LFSA microscope by using infrared differential
775 interference contrast (IR-DIC). To detect GFP fluorescence, a blue illumination was provided via a 470
776 nm LED and an ORCA-Flash4.0 LT digital CMOS camera (Hamamatsu) was used to collect images.
777 MetaMorph image acquisition software (Molecular Devices) was used to control the illumination and
778 camera. Analysis of imaging data was performed off-line using MetaMorph (Molecular Devices) and
779 Fiji software. Regions of interest (ROI) were drawn around individual tanycyte cell bodies from the
780 infrared and/or the fluorescence images. Changes in fluorescence intensity of GCaMP3 were
781 measured by plotting the intensity of ROI over time, after the intensity of a background ROI had been
782 subtracted. Then, an initial baseline fluorescence signal was computed before drug application at

783 resting state (F_0) and subsequent fluorescence values ($F-F_0=\Delta F$) were normalized to this ($\Delta F/F_0$).
784 Drugs were applied via puffs from a patch pipette made of borosilicate glass (World Precision
785 Instruments) and pulled on a P1000 puller (Sutter Instrument Co). The tip of the pipette was positioned
786 25 μm away from tanyocyte cell bodies. Puffs were delivered in the opposite direction of the flow of the
787 perfusion chamber at a pressure of 4 psi using a PV820 pneumatic PicoPump (World Precision
788 Instruments). The concentration of Leptin and ATP (Sigma) in the patch pipette was 6 μM and 10 mM
789 (both prepared in ACSF), respectively. To exclude mechanical responses of tanyocytes to the puff,
790 patch pipettes were also filled with ACSF alone.

791

792 ***Leptin receptor detection with the XPA antibody***

793 Twelve week-old C57Bl/6J mice were anesthetized with ketamine (8mg/kg body weight) + xylazine
794 (3mg/kg body weight) before being injected with the XPA antibody (2 nmol/animal, Xoma
795 Laboratories) into the jugular vein. As soon as the injection ended, mice were perfused with saline
796 (0,9% NaCl) and 4% paraformaldehyde. Brains were collected before being cryoprotected in 20%
797 sucrose solution overnight, embedded in Tissue Tek (Sakura®) and fresh-frozen. 20 μm -thick coronal
798 sections were cut and processed to reveal XPA using a 1 hour incubation at room temperature with
799 Biotinylated Goat anti-human IgG (1:1000; Jackson ImmunoResearch Labs Cat# 109-065-003,
800 RRID:AB_2337621). VECTASTAIN® Elite ABC peroxidase kit (PK-6100, Vector Laboratories) used
801 according to the manufacturer's instructions to amplify the signal. The XPA antibody was visualized
802 with a TSA Biotin Tyramide kit (SAT70001EA, Perkin Elmer) associated with Streptavidin Alexa
803 Fluor® 568 (1:600; Thermo Fisher Scientific Cat# S-11226, RRID:AB_2315774).

804

805 ***Proximity Ligation Assay***

806 Brain sections were fixed in 4% paraformaldehyde for 15 min, permeabilized and saturated with Triton
807 X100 (0.3%) and 5% Horse Serum/PBS solution for 1 h. Sections were incubated with primary
808 antibodies XPA (Xoma Laboratories) and rabbit anti-EGFR (Sigma, Ab-1070) at 4 °C overnight. PLA
809 was performed using a Duolink® In Situ Red Starter Kit Goat/Rabbit (Sigma-Aldrich) according to the
810 manufacturer's protocol. To assess the specificity of the PLA signal, the whole process was performed
811 with only one primary antibody.

812

813 ***RNAscope fluorescent in situ hybridization***

814 FISH was performed on 2% paraformaldehyde perfused brain sections (*Egfr*) and frozen brain
815 sections (*LepR*) of the median eminence of adult male mice using the RNAscope® Multiplex
816 Fluorescent Kit v2 according to the manufacturer's protocol (Advanced Cell Diagnostics, Inc., Newark,
817 CA, USA). Specific probes were used to detect *LepR* variant 1 (471171, NM_146146.2 , target region
818 3220 - 4109), *LepR* variant 3 (496901-C3 , NM_001122899.1 , target region 3291 - 4713), and *Egfr*
819 (443551-C2 , NM_207655.2 , target region 58-2111) mRNAs. Hybridization with a probe against the
820 *Bacillus subtilis* dihydrodipicolinate reductase (*dapB*) gene (320871) was used as a negative control.
821 Following *Egfr* FISH, vimentin immunolabeling was carried out using a chicken anti-Vimentin antibody
822 (1:500 Millipore Cat# AB1620, RRID:AB_90774), revealed with Goat anti-chicken 647 (1:500 ; Thermo
823 Fisher Scientific Cat# A-21449, RRID:AB_2535). For FISH experiments and immunofluorescence
824 labeling of Vimentin, the acquisition of images was performed using an inverted confocal microscope
825 (LSM 710, Zeiss, Jena, Germany). Excitation wavelengths of 493/562 nm, 568/643 and 640/740 were
826 selected to image Alexa 488- and Alexa 568-secondary antibodies and TSA plus Fluorescein, Cyanine
827 3 and Cyanine 5. UV laser (wavelength of 355 nm) was used to image Hoechst and DAPI. Z-stack
828 images were acquired with a W Plan-APOCHROMAT 20x objective (NA 0.5, zoom 1.0). High
829 magnification photomicrographs were acquired with a 63x objective (NA 1.4) using the Airyscan
830 detector (Zeiss). Images to be used for figures were pseudocolored, adjusted for brightness and
831 contrast and merged using Photoshop (Adobe Systems, San Jose, CA).

832

833 ***pSTAT3 immunohistochemistry and analysis***

834

835 Adult mice were sacrificed by decapitation in the morning at lights on. Brains were collected before
836 being embedded in Tissue Tek (Sakura®) and frozen freshly. 20 µm-thick coronal sections were cut,
837 postfixed with a solution of 2% paraformaldehyde during one hour and processed for
838 immunofluorescence as previously described (Bouret et al., 2012) using rabbit anti-pSTAT3 (Tyr705)
839 (1:1000; Cell Signaling Technology Cat# 9131, RRID:AB_331586) primary antibodies and revealed
840 with Goat anti-rabbit 647 (1/500; Molecular Probes Cat# A-21244, RRID:AB_141663).
841 Immunofluorescence images were acquired using an Axio Imager.Z2 Apotome microscope (AxioCam

842 MRm camera, Zeiss). Slides were then coded to conceal treatment groups, and pSTAT3
 843 immunoreactive (IR) cells counted in eight sections par animal.

844 ***Pancreatic Islet Studies***

845 Pancreata were digested by type V collagenase (C9263; 1,5 mg/ml) for 11 min at 37°C as described
 846 previously (Annicotte et al., 2009, Rabhi et al., 2016). Briefly, after digestion and separation in a
 847 density gradient medium, islets were purified by handpicking under microscope and cultured
 848 overnight in a 1640 RPMI (Gibco, 61870-010) media containing 1mM of FBS (Gibco, 10270-106) and
 849 Penicillin/streptomycin. For insulin secretion tests, approximately thirty islets were exposed to either
 850 2,8 mM or 20 mM glucose in Krebs-Ringer bicarbonate HEPES buffer containing 0,5% fatty-acid-free
 851 BSA. Insulin released in the medium was measured 1 hour later using the Ultrasensitive Insulin ELISA
 852 kit (Mercodia). Data are expressed as a ratio of total insulin content..

853 ***RNA Extraction, Measurements and Profiling of pancreatic islets***

854 Total RNA was extracted from islets using RNeasy Plus Micro Kit (Qiagen, Tokyo, Japan) according to
 855 the manufacturer's recommendations. mRNA expression was measured after reverse transcription by
 856 real-time qPCR with FastStart SYBR Green master mix (Roche) according to the manufacturer's
 857 recommendations and gene-specific oligonucleotides. Real-time qPCR results were normalized to
 858 endogenous cyclophilin reference mRNA levels. Results are expressed as the relative mRNA level of
 859 a specific gene expression using the formula $2^{-\Delta Ct}$. List of used primers are summarized in the table
 860 below.

Gene	Sense Primer	Antisense Primer
Cyclophiline	ATGGCACTGGCGGCAGGTCC	TTGCCATTCTGGACCCAAA
Glut2	AACCGGGATGATTGGCATGT	GGCGAATTTATCCAGCAGCA
Gck	GCTCAGTGAACCCCGGTCAGC	TGTGCGCAGCTGCTCTGAGG
Kcnj11	CACAAGCTGGGTTGGGGGCTC	TGCCCTCAGCTGGGTTCTGC
Glp-1r	GTTTCCTCACGGAAGCGCCA	AAGGAACCTGGGGGCCCATC
Ins1	GCCAAACAGCAAAGTCCAGG	GTTGAAACAATGACCTGCTTGC
Pcsk1	TGATGATCGTGTGACGTGGG	GGCAGAGCTGCAGTCATTCT
Pcsk2	AAAGATGGCGCTGCAACAAG	TTGCCAGTGTTGAACAGGT
Pdx1	ATTGTGCGGTGACCTCGGGC	GATGCTGGAGGGCTGTGGCG
MafA	TCCGACTGAAACAGAAGCGG	CTCTGGAGCTGGCACTTCTC
Nkx2.2	GTGCAGGGAGTATTGGAGGC	GAAGGGCCAGAGGAGGAGA

Hnf1a	GGTGCGTGTCTACAACCTGGT	ACCGTACACCGTGGACCTTA
Ucn3	TGATGCCACCTACTTCCTG	CTGTGTTGAGGCAGCTGAAG
NeuroD1	CTTGGCCAAGAACTACATCTGG	GGAGTAGGGATGCACCGGGAA
ATF4	ATGGCCGGCTATGGATGAT	CGAAGTCAAACCTTTTCAGATCCATT
Xbp1t	GAGCAGCAAGTGGTGGATTT	CCGTGAGTTTTCTCCCGTAA
Xbp1s	GAGTCCGCAGCAGGTG	GTGTCAGAGTCCATGGGA
ChOP	CTGCCTTTCACCTTGGAGAC	CGTTTCCTGGGGATGAGATA
Ero1b	GGGCCAAGTCATTAAGGAA	TTTATCGCACCCAACACAGT
PPP1R15a	GAGATTCCTCTAAAAGCTCGG	CAGGGACCTCGACGGCAGC
Pdia4	AGTCAAGGTGGTGGTGGAAAG	TGGGAGCAAATAGATGGTAGGG
Edem1	AAGTCTCAGGAGCTCAGAGTCATTA	CGATCTGGCGCATGTAGATG

861

862

863 ***Immunofluorescence (IF) on pancreatic sections***

864 IF was performed as described previously (Annicotte et al., 2009, Blanchett et al., 2011). Briefly, after
865 antigen retrieval using citrate buffer (Sigma) 5 µm formalin fixed pancreatic sections were incubated
866 with primary antibodies: Anti-Insulin (1:1000, Agilent Cat# A0564, RRID:AB_10013624), anti-Glucagon
867 (1:1000, Sigma-Aldrich Cat# G2654, RRID:AB_259852). Immunofluorescence stainings were revealed
868 using Goat Alexa 594-conjugated anti Guinea-Pig antibody (1:500, Molecular Probes Cat# A-11076,
869 RRID:AB_141930) and Goat Alexa 488-conjugated anti-Mouse (1:500, Thermo Fisher Scientific Cat#
870 A-11001, RRID:AB_2534069). Nuclei were stained with Hoescht. For morphometric analysis, images
871 were processed by ImageJ software by an observer blinded to experimental groups.

872 ***Western Blot analysis on liver and WAT***

873 Tissues were homogenized using a TissueLyser II (Qiagen, Tokyo, Japan) in cold RIPA buffer
874 (containing 200 mMTris/HCl (pH 7.4), 130 mM NaCl, 10%(v/v) glycerol, 0.1%(v/v) SDS, 1%(v/v) Triton
875 X-100, 10 mM MgCl₂) with anti-proteases and anti-phosphatases (Sigma-Aldrich; St. Louis, MO). The
876 tissue lysates were centrifuged for 30 minutes at 18000 g in a microfuge at 4°C. Liver and White
877 Adipose Tissue total protein lysates were subjected to sodium–dodecyl sulfate–polyacrylamide gels
878 (SDS–PAGE), then electrotransferred on a PVDF membrane and probed successively with the
879 following antibodies: Hormone sensitive lipase/HSL: (Abcam Cat# ab45422, RRID:AB_2135367) ;
880 Phospho-HSL (Ser660) (Cell Signaling Technology Cat# 4126, RRID:AB_490997) ; Phospho-Acetyl-

881 CoA Carboxylase (Ser79) (Cell Signaling Technology Cat# 3661, RRID:AB_330337) ; Acetyl CoA
882 Carboxylase 1 : (Millipore Cat# 04-322, RRID:AB_673047) ; Lipoprotein lipase (LPL Antibody (H-53)):
883 (Santa Cruz Biotechnology Cat# sc-32885, RRID:AB_2234585) ; Fatty Acid Synthase antibody (FAS):
884 (Abcam Cat# ab128870, RRID:AB_11143436) ; CPT1A: (Abcam Cat# ab128568,
885 RRID:AB_11141632) ; GAPDH: (Millipore Cat# CB1001, RRID:AB_2107426) ; β -actin: (Sigma-Aldrich
886 Cat# A2228, RRID:AB_47669) after incubating the membranes with 5% BSA blocking buffer. For
887 protein detection we used horseradish-peroxidase-conjugated secondary antibodies (Dako Denmark,
888 Glostrup, Denmark). Specific antigen-antibody bindings were visualized using chemiluminescence
889 method according to the manufacturer's instructions (Pierce ECL Western Blotting Substrate, Thermo
890 Scientific, USA). Values were expressed in relation to β -actin or GAPDH protein levels.

891 ***Blood lipids determinations***

892 Serum cholesterol levels (1001093, Spinreact), triglycerides levels (1001310, Spinreact), free fatty
893 acids levels (436-91995, 434-91795, WAKO) were measured by spectrophotometry in a
894 ThermoScientific Multiskan GO spectrophotometer.

895 ***Histomorphology of WAT***

896 WAT samples were fixed in 10% formalin for 24h and then were dehydrated and embedded in
897 paraffin. Sections of 3 μ m were made on a microtome and stained by the standard hematoxylin/eosin
898 alcoholic (BioOptica, Italy) and sections were observed and photographed using a Provis AX70
899 microscope (Olympus, Corp, Tokyo, Japan). Digital images were quantified with *ImageJ Software*
900 (National Institute of Health; USA).

901 ***Triglycerides content in liver***

902 Approx. 500mg of livers were homogenized for 3min in ice-cold chloroform-methanol (2:1, vol/vol).
903 Triglycerides were extracted during 3hours shaking at room temperature. For phase separation, mili-Q
904 water was added. Samples were centrifuged and the organic bottom layer was recollected. The
905 organic solvent was dried using a Speed Vac and re-dissolved in chloroform. Triglycerides content of
906 the samples were measured after evaporation of the organic solvent (1001310, Spinreact) by
907 spectrophotometry in a ThermoScientific Multiskan GO spectrophotometer.

908 ***Oil Red O Staining***

909 Frozen sections of 8 μ m of liver were cut with a cryostat and stained in filtered oil Red O for 10 min.
910 The sections were washed in distilled water, counterstained with Mayer's hematoxylin for 3 min, and

911 mounted in aqueous mountant. Sections were observed and photographed using a Provis AX70
912 microscope (Olympus, Corp, Tokyo, Japan).

913

914 **Primary cultures and cell lines experiments**

915 ***Primary culture of tanycytes***

916 Tanycytes were isolated from the median eminence of 10-day-old (P10) rats as described previously
917 ⁵⁴.

918 ***PamGene arrays***

919 Primary cultures of tanycytes were incubated at 37°C with leptin (125nM) or DMSO for 2 or 15 minutes
920 before washes and snap-freeze. For kinome analysis, STK microarrays were purchased from
921 PamGene International BV (STK pamchips). Sample incubation, detection, and analysis were
922 performed in a PamStation 12 according to the manufacturer's instructions and as previously
923 described (Rabhi et al., 2018).

924 ***Fluorescent leptin internalization assay and immunofluorescence on primary culture***

925 Tanycytes were seeded on poly-L-lysine-coated glass coverslips (10µg/ml) and incubated in TDM
926 (DMEM/F-12 (#11039, ThermoFisher), 1% L-glutamine (#25030-024, ThermoFisher), 2% penicillin-
927 streptomycin (#P4458, Sigma), insulin (1/1000, #I5500, Sigma), putrescin (1/500, #P5780, Sigma)) for
928 24 hours before the experiment. Tanycytes were incubated for the indicated amount of time at 37°C
929 with either bioactive fluorescent leptin (Fluorescent-leptin, 125 nM, Cisbio Bioassays) or with
930 fluorescent leptin antagonist (LAN, 125 nM, Cisbio Bioassays) both diluted in TDM. Cells were then
931 fixed for 10min at 4°C with 4% paraformaldehyde (PFA, v/v in PBS) and washed 3 times with PBS 1X.
932 For cointernalization assay, tanycytes were incubated with Fluorescent-leptin and XPA antibodies
933 (30nM in TDM, Xoma Laboratories) for 5 min, washed and fixed. Cells were then washed and
934 permeabilized with 0.1 % Triton-X100 (v/v in PBS) for 5 min at room temperature. Antibodies were all
935 diluted in PBS with 3% BSA and incubated for 45 min at room temperature. Cells were either
936 incubated with primary anti-EEA1 antibodies (1/200; Santa Cruz Biotechnology Cat# sc-6415,
937 RRID:AB_2096822) followed by the Alexa488-conjugated anti-goat antibodies (1/1000; Molecular
938 Probes Cat# A-11055, RRID:AB_2534102) or Alexa488-conjugated anti-human antibodies (1/1000;
939 Molecular Probes Cat# A-11013, RRID:AB_141360) to stain XPA antibodies.

940 ***Fluorescent leptin release assay on primary culture***

941 Tanycytes were incubated for 15 min at 37°C with either Fluorescent-leptin (125 nM, Cisbio
942 Bioassays) or LAN (125 nM ; Cisbio Bioassays). Cells were washed with TDM, incubated with TDM for
943 the indicated amount of time and fixed for 10 min at 4°C with 4% PFA. To assess the role of MAPK
944 pathway, tanycytes were pre-incubated for 30 min with the MAPK inhibitor UO126 (10 µM in TDM;
945 #9903; Cell signaling technology). Fluorescent-leptin uptake and release was performed in the
946 presence of UO126. To check for LAN release with EGF, EGF-TRITC (10 ng/ml; #3481; Molecular
947 probes) was added during the chase.

948 ***ELISA***

949 To quantify leptin release, tanycytes were cultivated in 10 cm Petri dish and incubated with
950 recombinant leptin (62.5 nM, Protein Rehovot Laboratory) diluted in TDM for 15 min at 37°C. Cells
951 were then washed and incubated with TDM to chase leptin for the indicated amount of time. Leptin in
952 the medium as well as leptin remaining in cells were quantified by Elisa assay according to the
953 manufacturer's instruction (#MOB00 ; R&D systems). Leptin secretion was expressed as a percent of
954 total leptin.

955

956 ***Image acquisition and analysis***

957 Cells were observed under a confocal microscope TCS SP5 (Leica microsystems) and images were
958 acquired according to Nyquist parameters using a 63x (NA 1.4) oil immersion objective. Single plane
959 images were analyzed using the open source Icy software (<http://icy.bioimageanalysis.org/>). The cell
960 periphery was manually delineated using phase contrast images and object-based segmentation using
961 wavelet transform algorithm (spot detector plugin) was performed to detect vesicles in each channel.
962 Objects were considered colocalized if the distance between their centroid was less than or equal to 3
963 pixels. EEA1 segmentation was used to estimate amounts of Leptin in EEA1 compartments and
964 percent of total leptin in EEA1 determined by normalizing the integrated intensity of leptin in EEA1 to
965 total leptin in cells.

966 ***Cells lines***

967 HEK293T (human embryonic kidney), HeLa (cervical cancer), CHO (Chinese hamster ovary) and N46
968 hypothalamic cells were grown in DMEM (Dulbecco's modified Eagle's medium; Gibco, life

969 technologies) with 4500 mg/l glucose and 10% fetal calf serum (Invitrogen) in a 10% CO₂ humidified
970 atmosphere at 37°C. HEK293T cells were transiently transfected (48h) with jetPEI (Polyplus-
971 transfection), with a mock pCDNA3 vector or LepR or EGFR expressing pCDNA3 plasmids, or with
972 LIFR- or IL6R-expressing pMET7 plasmids. Activation of the ERK signaling pathway was performed in
973 transfected HEK29T cells expressing exogenous EGFR, LepRb or both receptors, with or without a 1h
974 pretreatment with 1µM AG1478 inhibitor (T4182, Sigma) prior to 15min of stimulation with EGF (1nM),
975 Leptin (10nM) or both.

976 *Western Blot on primary cultures and cell lines*

977 The sequences and protocols for the preparation of the extracellular sub-domains of LepR have been
978 described previously by us ⁸⁰. Cell lysates (in Laemmli buffer supplemented with 30mM DTT, 2mM
979 orthovanadate and 10mM NaF) were separated by SDS/PAGE, transferred to nitrocellulose
980 membranes and immunoblotted with anti-phospho-tyrosine (Tyr-705) STAT3 (Cell Signaling
981 Technology Cat# 9145, RRID:AB_2491009) and anti-STAT3 antibodies (Cell Signaling Technology
982 Cat# 9139, RRID:AB_331757), anti-phospho-tyrosine (Tyr-204) ERK1/2 (Santa Cruz Biotechnology
983 Cat# sc-16982, RRID:AB_2139990) and anti-ERK2 (Proteintech Cat# 51068-1-AP,
984 RRID:AB_2250380) antibodies, anti-FLAG tag (Sigma-Aldrich Cat# SAB4301135,
985 RRID:AB_2811010), anti-HA tag (Cell Signaling Technology Cat#3724) or XPA (Xoma Laboratories).
986 Western Blots were scanned on the Odyssey infra-red Imaging System (Licor).

987

988 ***Co-Immunoprecipitation***

989 HEK293T cells were transfected with a Flag-EGFR-expressing vector either with LepR-YFP or an
990 empty vector. 48h later, cells were harvested in lysis buffer containing Tris-EDTA-magnesium-1%
991 Triton X-100 and solubilized for 2 hr (4°C, under rotation), centrifuged (14,000× g, 45 min), and
992 supernatants were subjected to immunoprecipitation with 2 µg of antibody anti-GFP (Roche); 4 hr,
993 4°C, under rotation. Protein G beads (Sigma-Aldrich) were then added, and after a 2 hr incubation, the
994 samples were washed in the 0.1% Triton X-100 buffer by repeated centrifugation (1,000× g, 5 min).
995 The remaining pellet was resuspended in Laemmli buffer (62.5-mM Tris/HCl pH 6.8, 5% SDS, 10%
996 glycerol, and 0.005% bromophenol blue), denaturated by heating (95°C, 5 min), and subjected to
997 SDS-PAGE analysis.

998

999 ***Bioluminescence resonance energy transfer (BRET)-based LepR biosensor***

1000 HEK293T cells were transiently transfected in 12-well plates with 40 ng of LepR-Luciferase plasmid
1001 with increasing amounts of LepR-YFP plasmids. Cells were grown overnight and transferred into 96-
1002 well-Optiplates (PerkinElmer Life Sciences), pre-coated with 10 µg/mL poly-l-lysine (Sigma), where
1003 they were grown for additional 24 h. The next day cells were stimulated with leptin, XPA or vehicle for
1004 30min at 37°C. After washing with PBS, Coelenterazine (Interchim France), a Luciferase substrate
1005 was added and cells were subjected to measurement of emission at Luciferase and YFP wavelength
1006 on a plate reader Tecan F500 (Tecan; Männedorf, Switzerland).

1007 ***TR-FRET binding assay***

1008 TR-FRET assays are based on the energy transfer between a fluorescently labeled donor molecule
1009 (the long-lived fluorophore Terbium cryptate (Tb)) and a fluorescently labeled acceptor (d2). In order to
1010 covalently label cell surface EGFR or LepR, with the Tb, the receptor is fused to the SNAP enzyme
1011 that can be covalently labeled with the Tb fluorophore at a stoichiometry of 1Tb per 1SNAP-receptor,
1012 using a suicide enzyme substrate-Tb. 48 hours post-transfection, HEK293T cells, expressing SNAP-
1013 EGFR +LepR or SNAP-LepR +EGFR, and previously plated in P96-well plates pre-coated with
1014 10 µg/mL poly-l-lysine (Sigma), are incubated with 100 nM of Tb-SNAP substrate in Tag-lite labeling
1015 medium (Cisbio Bioassays; 1h, 4°C). After several washes, cells are treated with several doses of
1016 leptin-d2 or EGF-d2 (CisbioAssays) respectively. For each concentration, non-specific binding was
1017 determined by adding an excess of unlabeled leptin or unlabeled EGF (200-500nM). Regarding the
1018 binding data analysis, the B_{max} signal and the equilibrium dissociation constant (K_D) values were
1019 obtained by fitting the specific binding data points (triplicate) with one-binding site model using the
1020 GraphPad Prism software (GraphPad Software, Inc., San Diego, CA).

1021

1022 **Statistics**

1023 Results are given as mean ± standard error mean (SEM). Samples or animals were excluded whether
1024 their values were outside the ± 2-fold standard deviation, or whether an objective experimental failure
1025 was observed; studies were not blinded to investigators or formally randomized. To test if the
1026 populations follow a Gaussian distribution, a normality test was performed (Kolmogorov-Smirnov test
1027 for n between 5-7; Shapiro-Wilk test for $n \geq 7$). For normal distributions, parametric test were used; for

1028 two population comparisons, an unpaired t tests was used as indicated in figure legends⁸¹⁻⁸³⁸¹⁻⁸³⁸¹⁻⁸³⁸⁰⁻
1029 ⁸²⁷⁹⁻⁸¹⁷⁸⁻⁸⁰⁷⁷⁻⁷⁹⁷⁶⁻⁷⁸⁷⁶⁻⁷⁸, for multiple comparison test, a one-way or two-way ANOVA followed by Tukey's
1030 *post hoc* multiple comparison test (unless otherwise indicated in the figure legends), was performed.
1031 For non-Gaussian distributions was used; Mann-Whitney test were used for two comparison test, and
1032 Kruskal-Wallis followed by Dunn *post hoc* test for multiple comparison. Data analysis was performed
1033 using GraphPad Prism Software Version 7 (GraphPad, San Diego, CA). The threshold for significance
1034 was $p < 0.05$.

1035

1036 REFERENCES

1037

- 1038 1. Swinburn, B.A., *et al.* The Global Syndemic of Obesity, Undernutrition, and Climate Change:
1039 The Lancet Commission report. *Lancet* **393**, 791-846 (2019).
- 1040 2. Yoon, K.H., *et al.* Epidemic obesity and type 2 diabetes in Asia. *Lancet* **368**, 1681-1688
1041 (2006).
- 1042 3. Ohn, J.H., *et al.* 10-year trajectory of beta-cell function and insulin sensitivity in the
1043 development of type 2 diabetes: a community-based prospective cohort study. *Lancet*
1044 *Diabetes Endocrinol* **4**, 27-34 (2016).
- 1045 4. Ahima, R.S. & Flier, J.S. Leptin. *Annu Rev Physiol* **62**, 413-437 (2000).
- 1046 5. de Luca, C., *et al.* Complete rescue of obesity, diabetes, and infertility in db/db mice by
1047 neuron-specific LEPR-B transgenes. *J Clin Invest* **115**, 3484-3493 (2005).
- 1048 6. Cohen, P., *et al.* Selective deletion of leptin receptor in neurons leads to obesity. *J.Clin.Invest*
1049 **108**, 1113-1121 (2001).
- 1050 7. Caron, A., Lee, S., Elmquist, J.K. & Gautron, L. Leptin and brain-adipose crosstalks. *Nat Rev*
1051 *Neurosci* **19**, 153-165 (2018).
- 1052 8. Pan, W.W. & Myers, M.G., Jr. Leptin and the maintenance of elevated body weight. *Nat Rev*
1053 *Neurosci* **19**, 95-105 (2018).
- 1054 9. Friedman, J.M. Leptin and the endocrine control of energy balance. *Nature Metabolism* **1**,
1055 754-764 (2019).
- 1056 10. Kamohara, S., Burcelin, R., Halaas, J.L., Friedman, J.M. & Charron, M.J. Acute stimulation of
1057 glucose metabolism in mice by leptin treatment. *Nature* **389**, 374-377 (1997).
- 1058 11. Coppari, R., *et al.* The hypothalamic arcuate nucleus: a key site for mediating leptin's effects
1059 on glucose homeostasis and locomotor activity. *Cell Metab* **1**, 63-72 (2005).
- 1060 12. Buettner, C., *et al.* Critical role of STAT3 in leptin's metabolic actions. *Cell Metab* **4**, 49-60
1061 (2006).
- 1062 13. Buettner, C., *et al.* Leptin controls adipose tissue lipogenesis via central, STAT3-independent
1063 mechanisms. *Nat Med* **14**, 667-675 (2008).
- 1064 14. Prevot, V., *et al.* The Versatile Tanycyte: A Hypothalamic Integrator of Reproduction and
1065 Energy Metabolism. *Endocr Rev* **39**, 333-368 (2018).
- 1066 15. Garcia-Caceres, C., *et al.* Role of astrocytes, microglia, and tanycytes in brain control of
1067 systemic metabolism. *Nat Neurosci* **22**, 7-14 (2019).
- 1068 16. Banks, W.A. The blood-brain barrier as an endocrine tissue. *Nat Rev Endocrinol* **15**, 444-455
1069 (2019).
- 1070 17. Schaeffer, M., *et al.* Rapid sensing of circulating ghrelin by hypothalamic appetite-modifying
1071 neurons. *Proc Natl Acad Sci U S A* **110**, 1512-1517 (2013).
- 1072 18. Ciofi, P., *et al.* Brain-endocrine interactions: a microvascular route in the mediobasal
1073 hypothalamus. *Endocrinology* **150**, 5509-5519 (2009).
- 1074 19. Yulyaningsih, E., *et al.* Acute Lesioning and Rapid Repair of Hypothalamic Neurons outside
1075 the Blood-Brain Barrier. *Cell Rep* **19**, 2257-2271 (2017).
- 1076 20. Djogo, T., *et al.* Adult NG2-Glia Are Required for Median Eminence-Mediated Leptin Sensing
1077 and Body Weight Control. *Cell Metab* **23**, 797-810 (2016).

- 1078 21. Mullier, A., Bouret, S.G., Prevot, V. & Dehouck, B. Differential distribution of tight junction
1079 proteins suggests a role for tanycytes in blood-hypothalamus barrier regulation in the adult
1080 mouse brain. *J Comp Neurol* **518**, 943-962 (2010).
- 1081 22. Langlet, F., *et al.* Tanycytic VEGF-A Boosts Blood-Hypothalamus Barrier Plasticity and
1082 Access of Metabolic Signals to the Arcuate Nucleus in Response to Fasting. *Cell Metab* **17**,
1083 607-617 (2013).
- 1084 23. Balland, E., *et al.* Hypothalamic tanycytes are an ERK-gated conduit for leptin into the brain.
1085 *Cell Metab* **19**, 293-301 (2014).
- 1086 24. Yuan, X., Caron, A., Wu, H. & Gautron, L. Leptin Receptor Expression in Mouse Intracranial
1087 Perivascular Cells. *Front Neuroanat* **12**, 4 (2018).
- 1088 25. Yoo, S., Cha, D., Kim, D.W., Hoang, T.V. & Blackshaw, S. Tanycyte-Independent Control of
1089 Hypothalamic Leptin Signaling. *Front Neurosci* **13**, 240 (2019).
- 1090 26. Bhaskar, V., *et al.* An allosteric antibody to the leptin receptor reduces body weight and
1091 reverses the diabetic phenotype in the Lep(ob)/Lep(ob) mouse. *Obesity (Silver Spring)* **24**,
1092 1687-1694 (2016).
- 1093 27. Jo, Y.H., Chen, Y.J., Chua, S.C., Jr., Talmage, D.A. & Role, L.W. Integration of
1094 endocannabinoid and leptin signaling in an appetite-related neural circuit. *Neuron* **48**, 1055-
1095 1066 (2005).
- 1096 28. Irani, B.G., Le Foll, C., Dunn-Meynell, A. & Levin, B.E. Effects of leptin on rat ventromedial
1097 hypothalamic neurons. *Endocrinology* **149**, 5146-5154 (2008).
- 1098 29. Kusumakshi, S., *et al.* A Binary Genetic Approach to Characterize TRPM5 Cells in Mice.
1099 *Chem Senses* **40**, 413-425 (2015).
- 1100 30. Niv-Spector, L., *et al.* Identification of the hydrophobic strand in the A-B loop of leptin as major
1101 binding site III: implications for large-scale preparation of potent recombinant human and
1102 ovine leptin antagonists. *Biochem J* **391**, 221-230 (2005).
- 1103 31. Muller-Fielitz, H., *et al.* Tanycytes control the hormonal output of the hypothalamic-pituitary-
1104 thyroid axis. *Nat Commun* **8**, 484 (2017).
- 1105 32. Frayling, C., Britton, R. & Dale, N. ATP-mediated glucosensing by hypothalamic tanycytes. *J*
1106 *Physiol* **589**, 2275-2286 (2011).
- 1107 33. Auriou, J., *et al.* Gain of affinity for VEGF165 binding within the VEGFR2/NRP1 cellular
1108 complex detected by an HTRF-based binding assay. *Biochem Pharmacol* **158**, 45-59 (2018).
- 1109 34. Vauthier, V., *et al.* Design and validation of a homogeneous time-resolved fluorescence-based
1110 leptin receptor binding assay. *Anal Biochem* **436**, 1-9 (2013).
- 1111 35. Langlet, F., Mullier, A., Bouret, S.G., Prevot, V. & Dehouck, B. Tanycyte-like cells form a
1112 blood-cerebrospinal fluid barrier in the circumventricular organs of the mouse brain. *J Comp*
1113 *Neurol* **521**, 3389-3405 (2013).
- 1114 36. Howard, J.K. & Flier, J.S. Attenuation of leptin and insulin signaling by SOCS proteins. *Trends*
1115 *Endocrinol Metab* **17**, 365-371 (2006).
- 1116 37. Chmielewski, A., *et al.* Preclinical Assessment of Leptin Transport into the Cerebrospinal Fluid
1117 in Diet-Induced Obese Minipigs. *Obesity (Silver Spring)* **27**, 950-956 (2019).
- 1118 38. Balland, E., Chen, W., Tiganis, T. & Cowley, M.A. Persistent leptin signalling in the arcuate
1119 nucleus impairs hypothalamic insulin signalling and glucose homeostasis in obese mice.
1120 *Neuroendocrinology* (2019).
- 1121 39. Sukumaran, S., Xue, B., Jusko, W.J., Dubois, D.C. & Almon, R.R. Circadian variations in gene
1122 expression in rat abdominal adipose tissue and relationship to physiology. *Physiol Genomics*
1123 **42A**, 141-152 (2010).
- 1124 40. Tschop, M., Smiley, D.L. & Heiman, M.L. Ghrelin induces adiposity in rodents. *Nature* **407**,
1125 908-913 (2000).
- 1126 41. Schwartz, M.W., *et al.* Specificity of leptin action on elevated blood glucose levels and
1127 hypothalamic neuropeptide Y gene expression in ob/ob mice. *Diabetes* **45**, 531-535 (1996).
- 1128 42. Pelleymounter, M.A., *et al.* Effects of the obese gene product on body weight regulation in
1129 ob/ob mice. *Science* **269**, 540-543 (1995).
- 1130 43. Berglund, E.D., *et al.* Direct leptin action on POMC neurons regulates glucose homeostasis
1131 and hepatic insulin sensitivity in mice. *J Clin Invest* **122**, 1000-1009 (2012).
- 1132 44. Back, S.H. & Kaufman, R.J. Endoplasmic reticulum stress and type 2 diabetes. *Annu Rev*
1133 *Biochem* **81**, 767-793 (2012).
- 1134 45. Sohn, J.W., *et al.* Melanocortin 4 receptors reciprocally regulate sympathetic and
1135 parasympathetic preganglionic neurons. *Cell* **152**, 612-619 (2013).
- 1136 46. Muzumdar, R., *et al.* Physiologic effect of leptin on insulin secretion is mediated mainly
1137 through central mechanisms. *FASEB J* **17**, 1130-1132 (2003).

- 1138 47. Fagerholm, V., Haaparanta, M. & Scheinin, M. alpha2-adrenoceptor regulation of blood
1139 glucose homeostasis. *Basic Clin Pharmacol Toxicol* **108**, 365-370 (2011).
- 1140 48. Rosengren, A.H., *et al.* Overexpression of alpha2A-adrenergic receptors contributes to type 2
1141 diabetes. *Science* **327**, 217-220 (2010).
- 1142 49. Wang, P., *et al.* A leptin-BDNF pathway regulating sympathetic innervation of adipose tissue.
1143 *Nature* **583**, 839-844 (2020).
- 1144 50. Ahima, R.S., *et al.* Role of leptin in the neuroendocrine response to fasting. *Nature* **382**, 250-
1145 252 (1996).
- 1146 51. Zhou, Y., *et al.* Temporal dynamic reorganization of 3D chromatin architecture in hormone-
1147 induced breast cancer and endocrine resistance. *Nat Commun* **10**, 1522 (2019).
- 1148 52. Liu, Z., *et al.* Short-term tamoxifen treatment has long-term effects on metabolism in high-fat
1149 diet-fed mice with involvement of Nmnat2 in POMC neurons. *FEBS Lett* **592**, 3305-3316
1150 (2018).
- 1151 53. Shida, D., Kitayama, J., Mori, K., Watanabe, T. & Nagawa, H. Transactivation of epidermal
1152 growth factor receptor is involved in leptin-induced activation of janus-activated kinase 2 and
1153 extracellular signal-regulated kinase 1/2 in human gastric cancer cells. *Cancer Res* **65**, 9159-
1154 9163 (2005).
- 1155 54. Prevot, V., Cornea, A., Mungenast, A., Smiley, G. & Ojeda, S.R. Activation of erbB-1 signaling
1156 in tanycytes of the median eminence stimulates transforming growth factor beta1 release via
1157 prostaglandin E2 production and induces cell plasticity. *J. Neurosci.* **23**, 10622-10632 (2003).
- 1158 55. Lomniczi, A., Cornea, A., Costa, M.E. & Ojeda, S.R. Hypothalamic tumor necrosis factor-alpha
1159 converting enzyme mediates excitatory amino acid-dependent neuron-to-glia signaling in the
1160 neuroendocrine brain. *J. Neurosci.* **26**, 51-62 (2006).
- 1161 56. Balthasar, N., *et al.* Leptin receptor signaling in POMC neurons is required for normal body
1162 weight homeostasis. *Neuron* **42**, 983-991 (2004).
- 1163 57. van de Wall, E., *et al.* Collective and individual functions of leptin receptor modulated neurons
1164 controlling metabolism and ingestion. *Endocrinology* **149**, 1773-1785 (2008).
- 1165 58. Vauthier, V., *et al.* Endospanin1 affects oppositely body weight regulation and glucose
1166 homeostasis by differentially regulating central leptin signaling. *Mol Metab* **6**, 159-172 (2017).
- 1167 59. Obici, S., *et al.* Central melanocortin receptors regulate insulin action. *J Clin Invest* **108**, 1079-
1168 1085 (2001).
- 1169 60. Fan, W., *et al.* The central melanocortin system can directly regulate serum insulin levels.
1170 *Endocrinology* **141**, 3072-3079 (2000).
- 1171 61. Rossi, J., *et al.* Melanocortin-4 receptors expressed by cholinergic neurons regulate energy
1172 balance and glucose homeostasis. *Cell Metab* **13**, 195-204 (2011).
- 1173 62. Coppari, R. & Bjorbaek, C. Leptin revisited: its mechanism of action and potential for treating
1174 diabetes. *Nat Rev Drug Discov* **11**, 692-708 (2012).
- 1175 63. Zamboni, M., Mazzali, G., Fantin, F., Rossi, A. & Di Francesco, V. Sarcopenic obesity: a new
1176 category of obesity in the elderly. *Nutr Metab Cardiovasc Dis* **18**, 388-395 (2008).
- 1177 64. Parr, E.B., Coffey, V.G. & Hawley, J.A. 'Sarcobesity': a metabolic conundrum. *Maturitas* **74**,
1178 109-113 (2013).
- 1179 65. Tian, S. & Xu, Y. Association of sarcopenic obesity with the risk of all-cause mortality: A meta-
1180 analysis of prospective cohort studies. *Geriatr Gerontol Int* **16**, 155-166 (2016).
- 1181 66. Okun, J.G., Rusu, P.M., Chan, A.Y. *et al.* Liver alanine catabolism promotes skeletal muscle
1182 atrophy and hyperglycaemia in type 2 diabetes. *Nat Metab* **3**, 394-409 (2021).
- 1183 67. Prentki, M. & Nolan, C.J. Islet beta cell failure in type 2 diabetes. *J Clin Invest* **116**, 1802-1812
1184 (2006).
- 1185 68. Steil, G.M., *et al.* Adaptation of beta-cell mass to substrate oversupply: enhanced function with
1186 normal gene expression. *Am J Physiol Endocrinol Metab* **280**, E788-796 (2001).
- 1187 69. Tuomi, T., *et al.* The many faces of diabetes: a disease with increasing heterogeneity. *Lancet*
1188 **383**, 1084-1094 (2014).
- 1189 70. Morimoto, A., *et al.* Impact of impaired insulin secretion and insulin resistance on the
1190 incidence of type 2 diabetes mellitus in a Japanese population: the Saku study. *Diabetologia*
1191 **56**, 1671-1679 (2013).
- 1192 71. Cohen, P., *et al.* Selective deletion of leptin receptor in neurons leads to obesity. *J Clin Invest*
1193 **108**, 1113-1121 (2001).
- 1194 72. Peitz, M., Pfannkuche, K., Rajewsky, K. & Edenhofer, F. Ability of the hydrophobic FGF and
1195 basic TAT peptides to promote cellular uptake of recombinant Cre recombinase: a tool for
1196 efficient genetic engineering of mammalian genomes. *Proc Natl Acad Sci U S A* **99**, 4489-
1197 4494 (2002).

- 1198 73. Folgueira, C., *et al.* Hypothalamic dopamine signaling regulates brown fat thermogenesis. *Nat*
1199 *Metab* **1**, 811-829 (2019).
- 1200 74. Quinones, M., *et al.* Sirt3 in POMC neurons controls energy balance in a sex- and diet-
1201 dependent manner. *Redox Biol* **41**, 101945 (2021).
- 1202 75. Bruss, M.D., Khambatta, C.F., Ruby, M.A., Aggarwal, I. & Hellerstein, M.K. Calorie restriction
1203 increases fatty acid synthesis and whole body fat oxidation rates. *Am J Physiol Endocrinol*
1204 *Metab* **298**, E108-116 (2010).
- 1205 76. Imbernon, M., *et al.* Central melanin-concentrating hormone influences liver and adipose
1206 metabolism via specific hypothalamic nuclei and efferent autonomic/JNK1 pathways.
1207 *Gastroenterology* **144**, 636-649 e636 (2013).
- 1208 77. Nogueiras, R., *et al.* The central melanocortin system directly controls peripheral lipid
1209 metabolism. *J Clin Invest* **117**, 3475-3488 (2007).
- 1210 78. Golde, W.T., Gollobin, P. & Rodriguez, L.L. A rapid, simple, and humane method for
1211 submandibular bleeding of mice using a lancet. *Lab Anim (NY)* **34**, 39-43 (2005).
- 1212 79. Clasadonte, J., Scemes, E., Wang, Z., Boison, D. & Haydon, P.G. Connexin 43-Mediated
1213 Astroglial Metabolic Networks Contribute to the Regulation of the Sleep-Wake Cycle. *Neuron*
1214 **95**, 1365-1380 e1365 (2017).
- 1215 80. Zabeau, L., *et al.* Selection of non-competitive leptin antagonists using a random nanobody-
1216 based approach. *Biochem J* **441**, 425-434 (2012).
- 1217 81. Student. The probable error of a mean. *Biometrika* **6**, 1-25 (1908).
- 1218 82. Fay, D.S. & Gerow, K. A biologist's guide to statistical thinking and analysis (). *WormBook :*
1219 *the online review of C. elegans biology*, 10.1895/wormbook.1891.1159.1891 (2013).
- 1220 83. Charan, J. & Biswas, T. How to Calculate Sample Size for Different Study Designs in Medical
1221 Research? *Indian Journal of Psychological Medicine* **35**, 121-126 (2013).

1222

1223

1224

ACKNOWLEDGMENTS

1225

1226

1227

1228

1229

1230

1231

1232

1233

1234

1235

1236

1237

1238

This work was supported by the Agence National de la Recherche (ANR, France) Grant ANR-15-CE14-0025 to VP, RJ and SG, « European Genomic Institute for Diabetes » (E.G.I.D, ANR-10-LABX-46 to JSA and VP), DISTALZ (ANR-11-LABX-0009 to VP), BETAPLASTICITY, ANR-17-CE14-0034 to JSA, Université de Lille (to MD, CB and JSA), Fondation pour la Recherche Médicale (FRM, to MD), European Foundation for the Study of Diabetes (EFSD, to JSA), the European Research Council (ERC) Synergy Grant-2019-WATCH-810331 to V.P., R. N. and M. S, the “Who am I?” laboratory of excellence No.ANR-11-LABX-0071 (to JD), the DHU Autoimmune and Hormonal Diseases (Authors) (JD), the H2020-MSCA-IF-2016 grant GLUCOTANYCYTES_748134 to MI and the NIH grant R01DK123002 to Y-BK and VP. We thank Laure Rolland for excellent technical help with immunofluorescence analysis of pancreatic sections. We thank Yann Lepage and the UMS2014-US41 for their technical support.

1237

1238

AUTHORS CONTRIBUTIONS

1239

1240

1241

1242

1243

1244

M.D., C.F., C.B., M.M., A.S., J.C., M.I., D.F., I.M.-C., S.K., E.C., E.I., N.J., A.O. and S.O carried out the experiments. M.M., J.T., E.T., M.S., S.K. and U.B. generated tools, vectors and animal models. Y.-B.K., R.J., M.S., U.B, R.N., J.-S.A., S.G., J.D. and V.P. designed and planned the study. All authors contributed to the preparation of the manuscript.

1243

1244

COMPETING INTERETS

1245

1246

The authors declare no competing interest.

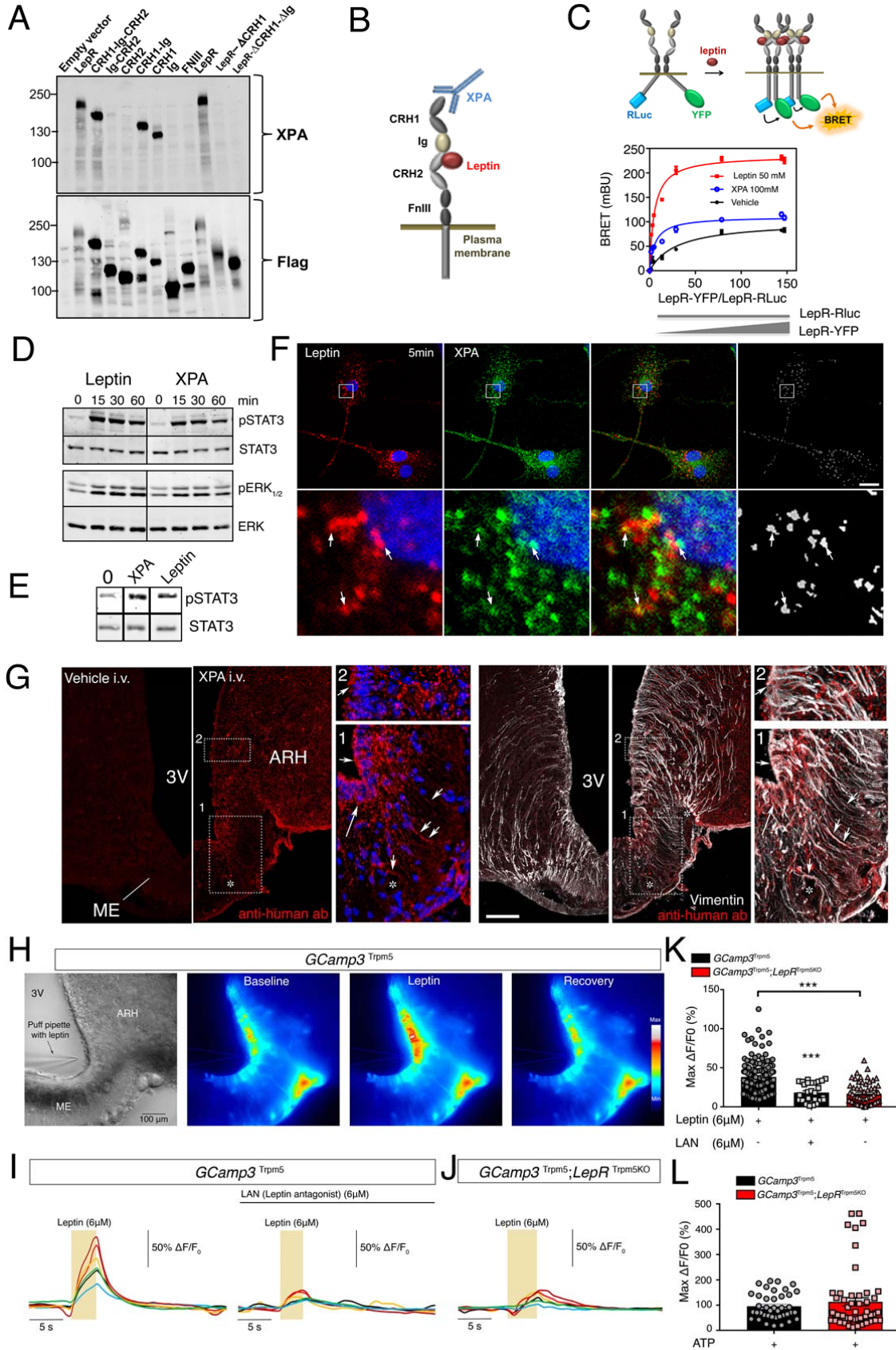
1246

1247

1248

1249

FIGURES



1252 **Figure 1. Tanycytes of the median eminence express functional leptin receptors**

1253 (A) Western blot detection using the XPA antibody of different exogenously expressed LepR domains
1254 in HEK293 cells.

1255 (B) Schematic representation of leptin receptor domains and the XPA binding site.

1256 (C) *Top*: schematic representation of the BRET assay to study the ligand-induced conformational
1257 change/interaction between LepR-RLuc and LepR-YFP. *Bottom*: BRET donor saturation curves in
1258 HEK293T cells with a constant expression level of LepR-RLuc and increasing levels of LepR-YFP,
1259 upon stimulation with vehicle, leptin (50nM) or XPA (100nM) for 30 min at 37 °C.

1260 (D) STAT3 and ERK1/2 phosphorylation in HEK293 cells stably expressing LepR after stimulation with
1261 50 nM leptin or 100 nM XPA for 5, 15, 30 or 60 minutes.

1262 (E) STAT3 phosphorylation in tanycytes upon 50 nM leptin or 100 nM XPA stimulation for 30 minutes.

1263 (F) Leptin colocalizes with LepR in primary tanycytes. Representative confocal images of tanycytes
1264 treated for 5 min with 125 nM fluorescent leptin (red) together with 33 nM XPA antibodies against
1265 LepR labeled with fluorescent secondary antibodies (green). The extent of colocalization is
1266 represented by the mask on the right. Arrows point to examples of colocalized pixels. Scale bar: 10
1267 μm .

1268 (G) Representative photomicrograph revealing sites of XPA fixation in tanycytes of the median
1269 eminence (vimentin-positive cells) 2 minutes after intravenous XPA injection (2 nmol/animal) *in vivo*.
1270 White arrows show XPA (red) and vimentin (white) colocalization. 3V: third ventricle; ARH: arcuate
1271 nucleus of the hypothalamus; ME: median eminence. Scale bar: 200 μm .

1272 (H) Representative image of a living brain slice containing the median eminence from a *GCamp3^{Trpm5}*
1273 mouse under bright-field and fluorescence microscopy, showing the reversible increase in intracellular
1274 calcium levels in tanycytic cell bodies lining the third ventricle (3V) upon the local application of a puff
1275 of leptin (6 μM) via a glass pipette. ME: median eminence. Scale bar: 100 μm

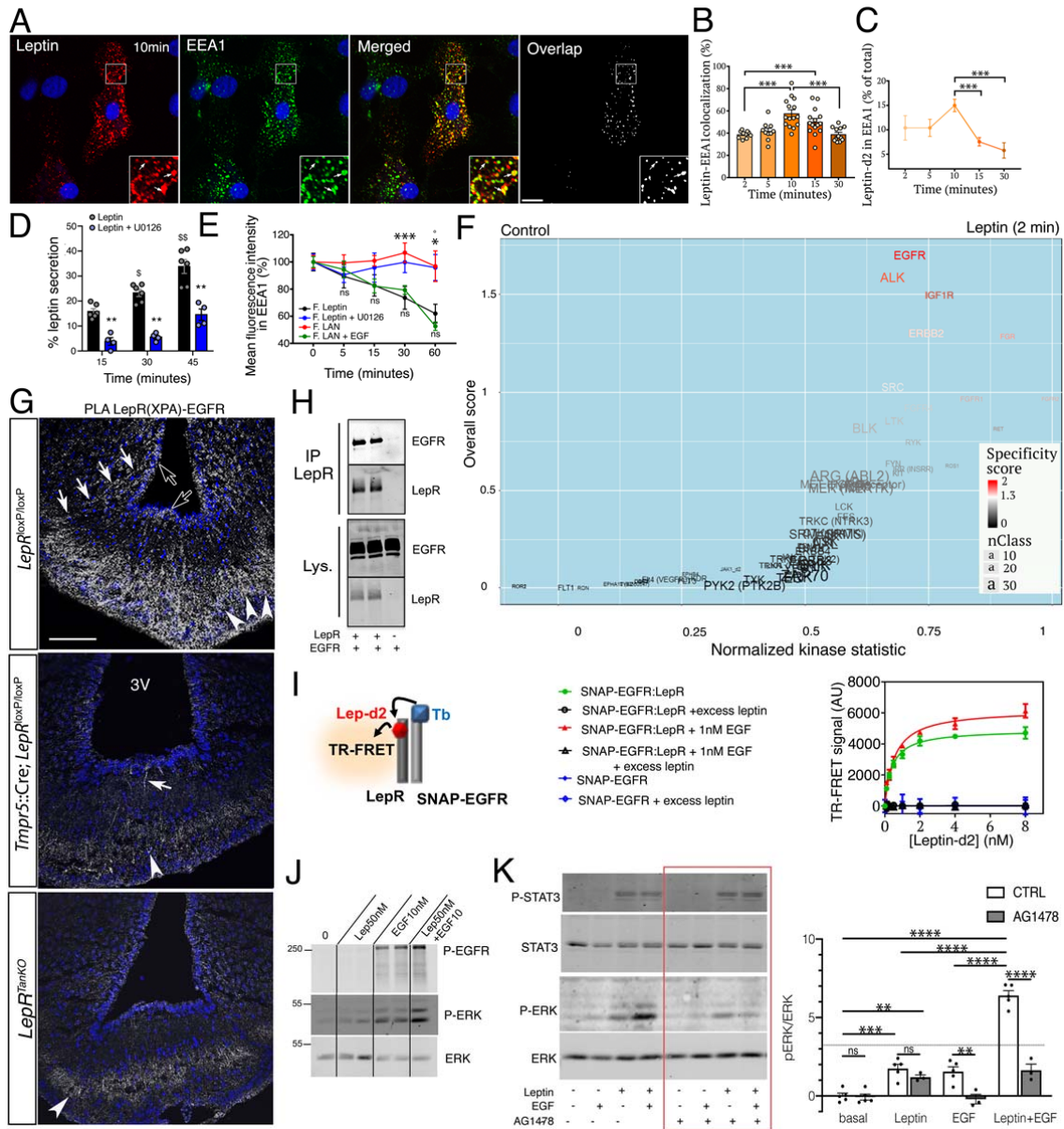
1276 (I) Representative curves of GCamp3 fluorescence (calcium current) over time (Delta T) compared to
1277 the baseline in tanycytes in living hypothalamic slices during a puff of leptin (yellow rectangle, 6 μM),
1278 alone (left curve) or after pre-treatment with leptin antagonist (LAN, 6 μM , top black line; right curve), in
1279 a *GCamp3^{Trpm5}* mouse.

1280 (J) Same measurement as in (I) in a *GCamp3^{Trpm5}; LepR^{Trpm5}* mouse lacking LepR in tanycytes after a
1281 puff of leptin (6 μM , yellow rectangle).

1282 (K) Graph representing maximum difference in calcium concentration from baseline during the
1283 treatment of living brain slices in *GCamp3^{Trpm5}* and *GCamp3^{Trpm5}; LepR^{Trpm5}* mice, described in (I) and
1284 (J). Mann Whitney test; ***: $p < 0.001$; between indicated groups. Values indicate means \pm SEM.

1285 (L) Graph representing maximum c difference in calcium concentration from baseline during a puff of
1286 ATP (10 mM) in living brain slices from *GCamp3^{Trpm5}* and *GCamp3^{Trpm5}; LepR^{Trpm5}* mice. See also
1287 Supplementary Figure 1.

1288



1289

1290

1291

Figure 2. Tancytic EGFR physically interacts with LepR *in vivo* and plays a role in leptin transcytosis *in vitro*

1292

1293

1294

1295

(A) Endocytosed leptin colocalizing with early endosomes. Representative confocal images showing primary tancytes treated for 10 min with 125 nM fluorescent leptin (red) and antibodies to the early endosome marker EEA1 (green). The extent of colocalization is represented by the mask on the right. Arrows in inset point to examples of colocalized pixels. Scale bar: 10 μ m.

1296

1297

1298

(B) Percentage of leptin colocalizing with EEA1 over time following object-based detection of fluorescent leptin and EEA1 vesicles. Values represent means \pm SEM. A Mann-Whitney test was applied. ***: $p < 0.001$

1299

1300

(C) Percentage of endocytosed leptin found in the EEA1-positive compartment over time. Values represent means \pm SEM. A Mann-Whitney test was applied. ***: $p < 0.001$

1301

1302

1303

1304

(D) Leptin secreted into the medium by primary cultures of tancytes as a percentage of total leptin concentration (intracellular and medium) 15, 30 and 45 minutes after fluorescent leptin addition. Mann-Whitney U test or one-way ANOVA as required. **: $p < 0.01$ leptin vs. leptin + U0126; \$: $p < 0.05$ Leptin 15 min vs. Leptin 30 min and \$\$: $p < 0.01$ Leptin 30 min vs. Leptin 45 min.

1305
1306 (E) Percentage (as % of 0 min time point) of endocytosed fluorescent leptin or fluorescent LAN found
1307 in EEA1 compartments over time in cells treated or not with U0126 (leptin) or EGF (LAN). Values
1308 represent means \pm SEM. A Mann-Whitney U test was applied. ***: $p < 0.001$

1309 (F) Volcano plot showing differences in peptide phosphorylation between primary cultures of tanycytes
1310 treated for 2 min with vehicle (PBS pH 8.0) or leptin (1 $\mu\text{g}/\text{ml}$ in PBS pH 8.0) ($n=4$). Upstream kinases
1311 were identified using the Human Protein Reference Database.

1312 (G) Proximity Ligation Assay (PLA) between LepR and EGFR using XPA and a rabbit anti-EGFR
1313 antibody. PLA signal is seen in tanycytic cell bodies (empty arrows), processes (white arrows) and
1314 end-feet in the external zone of the median eminence, where they contact the fenestrated endothelium
1315 of the pituitary portal circulation (arrowheads). Scale bar: 100 μm .

1316 (H) Co-immunoprecipitation of EGFR along with LepR in HEK293T cells; no co-immunoprecipitation of
1317 EGFR is observed when LepR is not expressed. IP, immunoprecipitation; Lys., cell lysate.

1318 (I) Schematic representation of the TR-FRET technique (left). Right: specific saturation curves of
1319 leptin-d2 binding to its cognate receptor LepR within the LepR:SNAP-EGFR complex at the cell
1320 surface are obtained after 3h at 37°C; no TR-FRET signal is detected when SNAP-EGFR is expressed
1321 in the absence of LepR. Saturation binding experiments are performed by adding an increasing dose
1322 of leptin-d2, combined or not with 1nM EGF, to HEK293 cells expressing SNAP-EGFR alone or in
1323 combination with LepR and pre-labeled with the fluorescent SNAP-Tb substrate. The TR-FRET signal
1324 is strongly displaced by an excess of unlabeled leptin (200nM). Data are presented as means \pm SD of
1325 3 replicates of 1 representative experiment out of 3 independent experiments. The mean dissociation
1326 constant was determined from the average of the K_d values extracted from a fitting analysis of the
1327 saturation curve of 3 independent experiments with non-linear regression "one-site specific binding
1328 equation.

1329 (J) Phosphorylation of EGFR and ERK upon addition of leptin 50nM, EGF 10nM or both for 30min at
1330 37°C in primary tanycytes.

1331 (K) Phosphorylation of STAT3 and ERK upon addition of leptin 10nM, EGF 1nM or both for 30min at
1332 37°C in HEK293T cells expressing endogenous EGFR and transfected with LepRb in the presence or
1333 absence of the EGFR inhibitor AG1478 (1 μM).

1334
1335

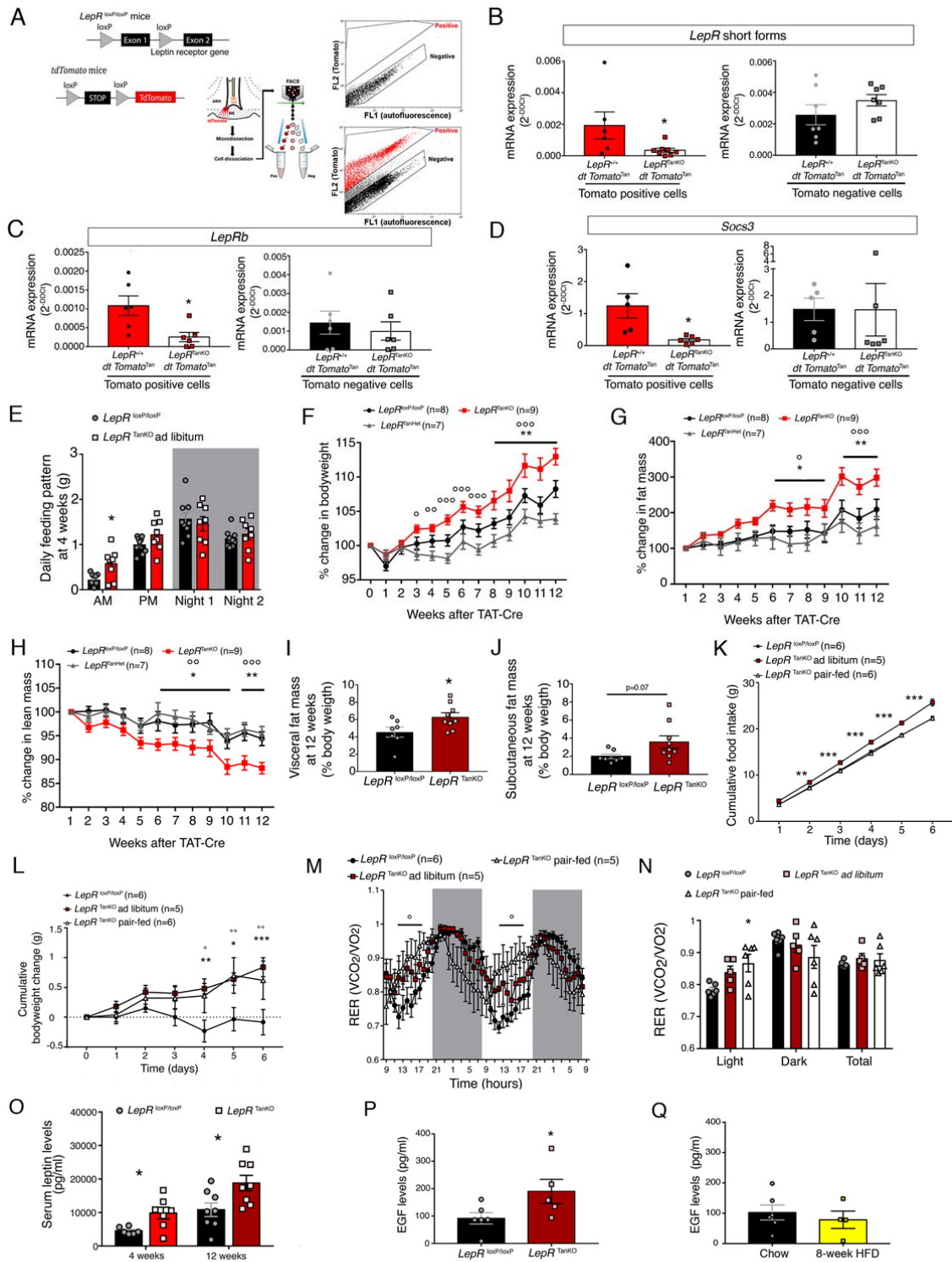
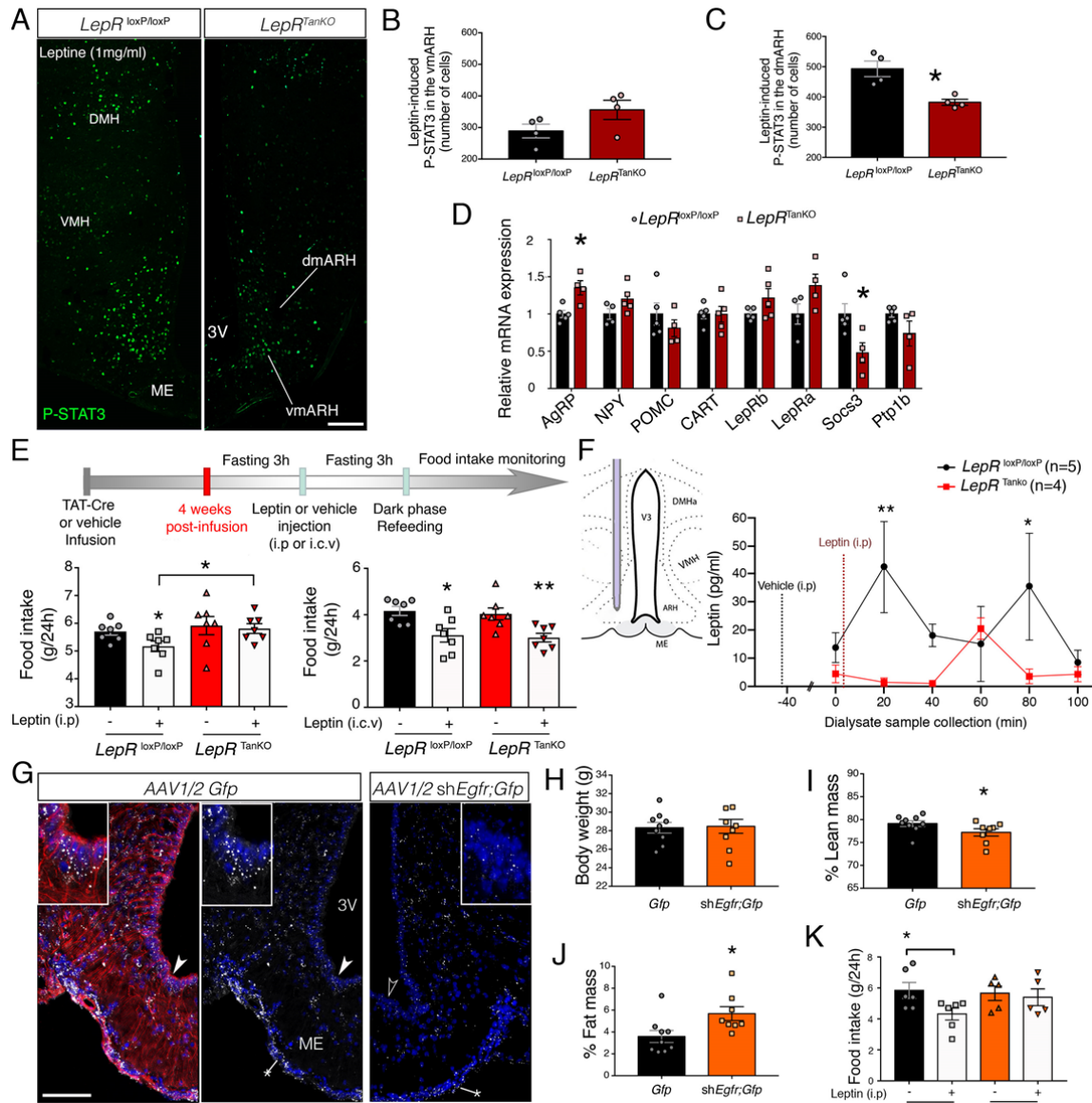


Figure 3. Selective LepR deletion in tanyocytes causes food-intake-independent body weight gain and increased adiposity

(A) Schematic diagram and gating strategy for sorting Tomato positive cells following vehicle (top panel) and TAT-Cre infusion (bottom panel) into the third ventricle (3V) of *LepR^{+/+}; tdTomato^{loxP-STOP-loxP}* or *LepR^{loxP/loxP}; tdTomato^{loxP-STOP-loxP}* littermates.

1343 (B-D) mRNA expression levels of short forms (B) and the long form, LepRb (C), of the leptin receptor,
1344 and of Socs3 (D) in tdTomato-positive cells (left panels) and tdTomato-negative cells (right panels). A
1345 Student t-test or Mann-Whitney U test was applied, depending on Shapiro-Wilk normality test results. *:
1346 $p < 0.05$; $LepR^{+/+}$ tdTomato^{Tan} vs. $LepR^{TanKO}$ tdTomato^{Tan}. Values indicate means \pm SEM.
1347
1348 (E) Food intake pattern (daily average of automatic measurements in metabolic cages over 24h),
1349 showing an increase at lights-on in $LepR^{TanKO}$ mice when compared to $LepR^{loxP/loxP}$ littermates. *: $p < 0.05$. Values indicate means \pm SEM. The night was divided in two 6h time slots (Night 1 and Night
1350 2).
1351
1352 (F-H) Curves representing the kinetics of the % change in body weight (F), % change in fat mass (G)
1353 and % change in lean mass (H) between $LepR^{loxP/loxP}$, $LepR^{TanHet}$ and $LepR^{TanKO}$ through the 12 weeks
1354 following the TAT-Cre infusion into the 3V. Two-way ANOVA with Tukey's correction; *: $p < 0.05$,
1355 $LepR^{loxP/loxP}$ vs. $LepR^{TanKO}$; **, $p < 0.01$, $LepR^{loxP/loxP}$ vs. $LepR^{TanKO}$; °: $p < 0.05$, $LepR^{TanHet}$ vs. $LepR^{TanKO}$;
1356 °°: $p < 0.01$, $LepR^{TanHet}$ vs. $LepR^{TanKO}$; °°°: $p < 0.05$, $LepR^{TanHet}$ vs. $LepR^{TanKO}$. Values represent means \pm
1357 SEM
1358
1359 (I,J) Visceral fat mass (I) and subcutaneous (J) 12 weeks after TAT-Cre infusion. Mann-Whitney U
1360 test; *: $p < 0.05$, $LepR^{loxP/loxP}$ vs. $LepR^{TanKO}$. Values indicate means \pm SEM.
1361
1362 (K) Cumulative food intake in $LepR^{TanKO}$ pair-fed mice 12 weeks after TAT-Cre infusion compared to
1363 their control littermates. 2-way ANOVA with Tukey's correction; **: $p < 0.01$, $LepR^{loxP/loxP}$ and $LepR^{TanKO}$
1364 pair-fed vs. $LepR^{TanKO}$ fed *ad libitum*; ***: $p < 0.001$, $LepR^{loxP/loxP}$ and $LepR^{TanKO}$ pair-fed vs $LepR^{TanKO}$ *ad*
1365 *libitum*. Values indicate means \pm SEM.
1366
1367 (L) Cumulative body weight change. 2-way ANOVA with Tukey's correction; *: $p < 0.05$, $LepR^{loxP/loxP}$ vs.
1368 $LepR^{TanKO}$ fed *ad libitum*; **: $p < 0.01$, $LepR^{loxP/loxP}$ vs. $LepR^{TanKO}$ fed *ad libitum*; ***: $p < 0.001$, $LepR^{loxP/loxP}$
1369 vs. $LepR^{TanKO}$ fed *ad libitum*; °: $p < p < 0.05$, $LepR^{loxP/loxP}$ vs. $LepR^{TanKO}$ pair-fed; °°: $p < p < 0.01$,
1370 $LepR^{loxP/loxP}$ vs. $LepR^{TanKO}$ pair-fed. Values indicate means \pm SEM.
1371
1372 (M) Energy ratio (RER) over time. 2-way ANOVA with uncorrelated Fisher's LSD test; °: $p < p < 0.05$,
1373 $LepR^{loxP/loxP}$ vs. $LepR^{TanKO}$ pair-fed. Values indicate means \pm SEM.
1374
1375 (N) Mean energy ratio (RER) during light phase, dark phase and total.
1376 Two-way ANOVA with Tukey's correction; *: $p < p < 0.05$, $LepR^{loxP/loxP}$ vs. $LepR^{TanKO}$ pair-fed. Values
1377 indicate means \pm SEM.
1378
1379 (O) Circulating leptin levels in $LepR^{loxP/loxP}$ and $LepR^{TanKO}$ animals at 4 weeks and 12 weeks after TAT-
1380 Cre infusion into the 3V. Mann-Whitney test (4 weeks) and unpaired t-test (12 weeks). *: $p < 0,05$
1381 $LepR^{loxP/loxP}$ vs. $LepR^{TanKO}$. Values represent means \pm SEM.
1382
1383 (P) Basal serum EGF concentrations in $LepR^{loxP/loxP}$ and $LepR^{TanKO}$ mice, 12 weeks after TAT-Cre
1384 infusion. Mann-Whitney U test. *: $p < 0.05$, $LepR^{loxP/loxP}$ vs. $LepR^{TanKO}$.
1385
1386 (Q) Basal serum EGF concentrations in C57Bl/6J mice fed normal chow or those fed a high-fat diet for
1387 8 weeks.
1388
1389
1390
1391



1394

1395 **Figure 4. Defective LepR and EGFR signaling in tanycytes causes hypothalamic resistance to**
1396 **circulating leptin.**

1397 (A-C) Representative photomicrograph (A) and quantification of leptin-induced P-STAT3
1398 immunofluorescence in the ventromedial (vm) (B) and dorsomedial (dm) arcuate nucleus (ARH) (C).
1399 Scale bar: 200µm. Unpaired Student's t-test. *: p<0.05 *LepR^{loxP/loxP}* vs *LepR^{TanKO}*. Values indicate
1400 means ± SEM.

1401 (D) Relative mRNA expression levels of several genes known to be involved in the hypothalamic
1402 regulation of energy homeostasis and leptin activity in the microdissected mediobasal hypothalamus
1403 (MBH) of *LepR^{loxP/loxP}* and *LepR^{TanKO}* mice, 12 weeks after TAT-Cre infusion. Student's t-test or Mann-
1404 Whitney U test, depending on Shapiro-Wilk normality test results. *: p<0.05, *LepR^{loxP/loxP}* vs. *LepR^{TanKO}*.
1405 Values indicate means ± SEM.

1406 (E) Schematic diagram showing the design of the experiment investigating the anorectic response to
1407 either intraperitoneal (i.p) or intracerebroventricular (i.c.v) leptin administration. Bottom left graph
1408 represents food intake in *LepR^{loxP/loxP}* (black and grey bars) and *LepR^{TanKO}* mice (red and pink bars)

1409 24h after i.p. leptin (3mg/kg, grey and pink bars) or vehicle (PBS pH 8.0, black and red bars)
1410 administration. Bottom right graph represents food intake in $LepR^{loxP/loxP}$ and $LepR^{TanKO}$ mice 24h after
1411 i.c.v. leptin (2µg in 2µL) or vehicle (2µL PBS pH 8.0) injection. Mann-Whitney U test; *: $p<0.05$; **: $p<0.01$;
1412 leptin vs. vehicle and between indicated groups. Values indicate means \pm SEM.

1413 (F) Leptin concentrations in the ARH interstitial liquid collected by microdialysis every 20 minutes
1414 following i.p. vehicle ($t_{40 \text{ min}}$) or leptin ($t_{1 \text{ min}}$) injection in $LepR^{loxP/loxP}$ (n= 7) and $LepR^{TanKO}$ mice (n=6).
1415 Two-way ANOVA followed by Fisher's LSD post hoc test analysis was applied; *: $p<0.05$; **: $p<0.01$;
1416 $LepR^{loxP/loxP}$ vs. $LepR^{TanKO}$

1417 (G) Representative photomicrograph of *in situ* hybridization of EGFR using RNAscope technology on
1418 fresh-frozen brain sections from the median eminence of C57Bl/6J mice injected with AAV1/2
1419 $Dio2::gfp$ or AAV(1+2)-GFP-U6-m-EGFR-shRNA. The left panel shows vimentin-immunoreactivity in
1420 red. Arrowheads show the cells seen at higher magnification in insets. Scale bar: 100µm (25 µm in
1421 inset).

1422 (H-J) Curves representing the evolution of body weight (H), % change in fat mass (I) and % change in
1423 lean mass (J) between mice injected with AAV1/2 $Dio2::gfp$ (control in black) or AAV(1+2)-GFP-U6-m-
1424 EGFR-shRNA (in orange) over 4 weeks following the beginning of the viral activity. 2-way ANOVA with
1425 Tukey's correction; *: $p<0.05$, AAV1/2 Gfp vs. AAV1/2 $shEgfr$.

1426 (K) Graph representing food intake in mice injected with AAV1/2 $Dio2::gfp$ or AAV(1+2)-GFP-U6-m-
1427 EGFR-shRNA 24h after i.p. leptin (1mg/kg) or vehicle (PBS pH 8.0) injection. An unpaired Student's t-
1428 test was applied; *: $p<0.05$; **: $p<0.01$; leptin vs. vehicle and between indicated groups. Values
1429 indicate means \pm SEM.

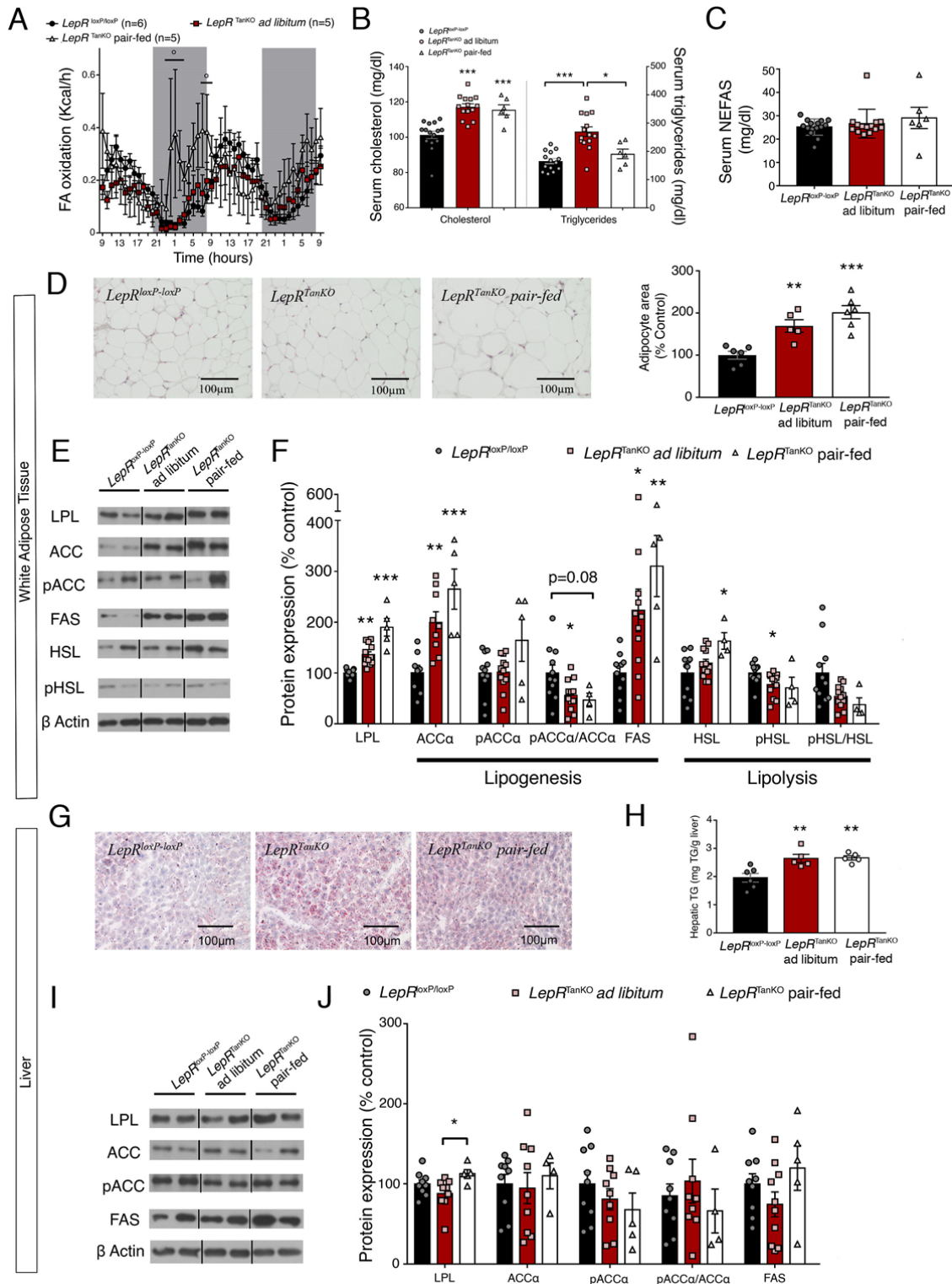


Figure 5: Selective LepR deletion in tancytes causes hyperlipidemia and steatosis

(A) Fatty-acid (FA) oxidation over time. 2-way ANOVA with uncorrelated Fisher's LSD test; °: $p < 0.05$, $LepR^{loxP/loxP}$ vs. $LepR^{TanKO}$ pair-fed. Values indicate means \pm SEM.

(B) Graphs representing serum cholesterol and triglyceride concentrations in $LepR^{loxP/loxP}$ and $LepR^{TanKO}$ mice fed *ad libitum* on chow and $LepR^{TanKO}$ mice pair-fed with $LepR^{loxP/loxP}$ mice, 12 weeks

1438 after TAT-Cre infusion. One-way ANOVA with Tukey multiple comparison test or Kruskal-Wallis test
1439 with Dunn multiple comparison test were applied depending Shapiro-Wilk normality test results.. *: $p < 0.05$;
1440 $p < 0.05$; ***: $p < 0.001$, $LepR^{TanKO}$ *ad libitum* or $LepR^{TanKO}$ pair fed vs. $LepR^{loxP/loxP}$ mice. Values indicate
1441 means \pm SEM.

1442 (C) Graph representing serum non-esterified fatty acid (NEFAS) concentrations in $LepR^{loxP/loxP}$ and
1443 $LepR^{TanKO}$ mice fed *ad libitum* on chow and $LepR^{TanKO}$ mice pair-fed with $LepR^{loxP/loxP}$ mice, 12 weeks
1444 after TAT-Cre infusion. One-way ANOVA with Tukey multiple comparison test *: $p < 0.05$; ***: $p < 0.001$,
1445 $LepR^{TanKO}$ *ad libitum* or $LepR^{TanKO}$ pair fed vs. $LepR^{loxP/loxP}$ mice. Values indicate means \pm SEM.

1446 (D) Representative images of histological hematoxylin-eosin staining of the adipose tissue in
1447 $LepR^{loxP/loxP}$ and $LepR^{TanKO}$ mice fed *ad libitum* on chow and $LepR^{TanKO}$ mice pair-fed with $LepR^{loxP/loxP}$
1448 mice. Graph shows quantification of adipocyte size. One-way ANOVA with Tukey multiple comparison
1449 test. **: $p < 0.01$, ***: $p < 0.001$, $LepR^{TanKO}$ *ad libitum* or $LepR^{TanKO}$ pair fed vs. $LepR^{loxP/loxP}$ mice. Values
1450 indicate means \pm SEM.

1451 (E) Representative western blots of the different proteins mentioned in (E).

1452 (F) Graph representing protein expression levels of several proteins implicated in fatty acid synthesis
1453 or fatty acid lipolysis in white adipose tissue from $LepR^{loxP/loxP}$ and $LepR^{TanKO}$ mice, 12 weeks after
1454 TAT-Cre infusion. Lipoprotein lipase (LPL) is implicated in the lipids uptake from the circulation to the
1455 adipose tissue. One-way ANOVA with Tukey multiple comparison test or Kruskal-Wallis test with Dunn
1456 multiple comparison test. *: $p < 0.05$; ***: $p < 0.001$, $LepR^{TanKO}$ *ad libitum* or $LepR^{TanKO}$ pair fed vs.
1457 $LepR^{loxP/loxP}$ mice. Values indicate means \pm SEM.

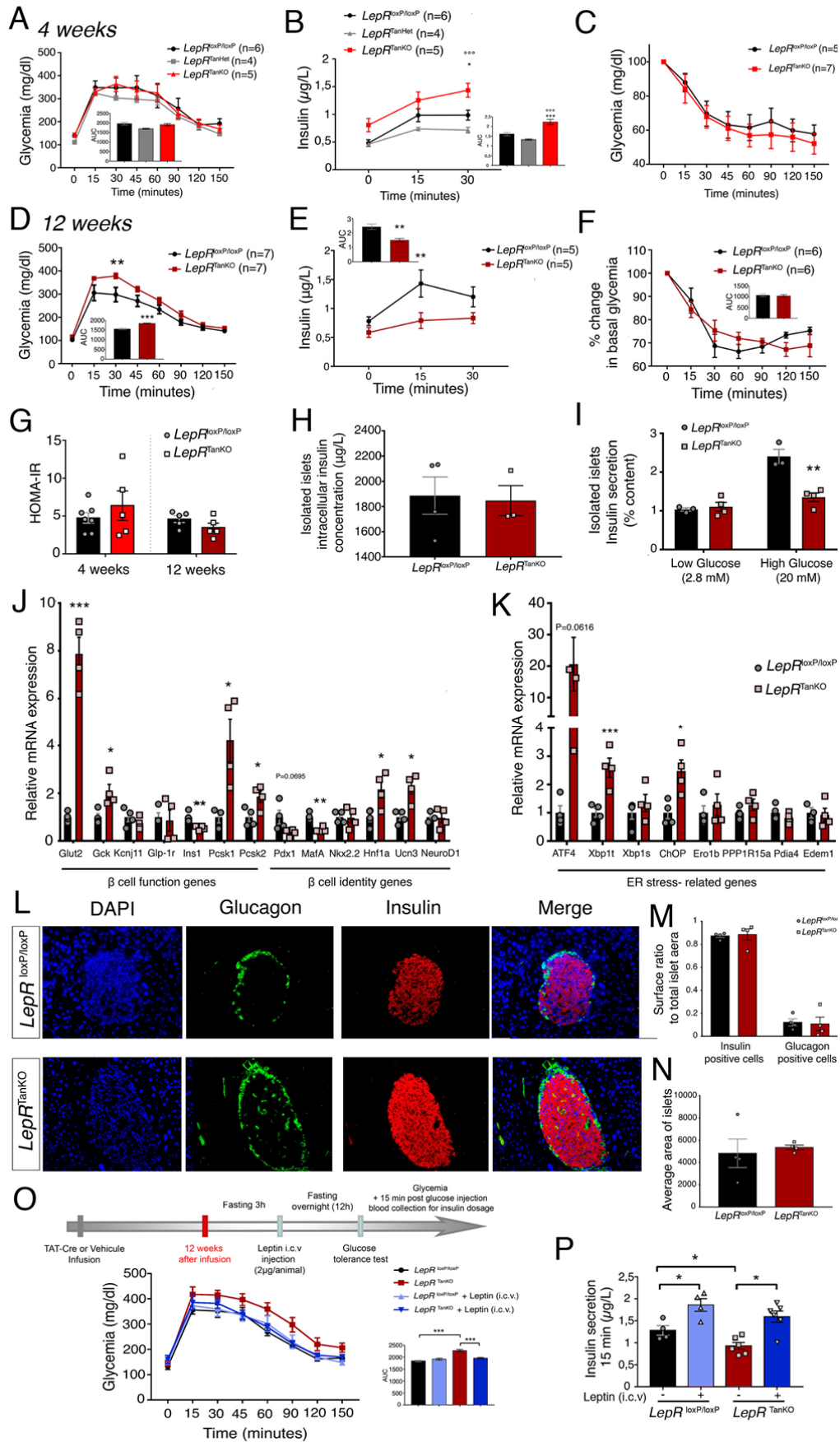
1458 (G) Representative Oil-Red-stained images from the liver of $LepR^{loxP/loxP}$ and $LepR^{TanKO}$ mice fed *ad*
1459 *libitum* and $LepR^{TanKO}$ mice pair-fed with $LepR^{loxP/loxP}$ mice.

1460 (H) Quantification of triglycerides in the liver of $LepR^{loxP/loxP}$ and $LepR^{TanKO}$ mice fed *ad libitum* and
1461 $LepR^{TanKO}$ mice paired-fed with $LepR^{loxP/loxP}$ mice. One-way ANOVA with Tukey multiple comparison
1462 test. **: $p < 0.01$, $LepR^{TanKO}$ *ad libitum* or $LepR^{TanKO}$ pair fed vs. $LepR^{loxP/loxP}$ mice. Values indicate
1463 means \pm SEM.

1464 (I) Representative western blots of the different proteins mentioned in (I).

1465 (J) Graph representing protein expression levels of several proteins implicated in fatty acid synthesis
1466 and lipid uptake from the circulation into the liver in $LepR^{loxP/loxP}$ and $LepR^{TanKO}$ mice fed *ad libitum* and
1467 $LepR^{TanKO}$ mice paired-fed with $LepR^{loxP/loxP}$ mice, 12 weeks after TAT-Cre infusion. One-way ANOVA
1468 with Tukey multiple comparison test. *: $p < 0.05$; $LepR^{TanKO}$ pair fed vs. $LepR^{TanKO}$ *ad libitum* mice.
1469 Values indicate means \pm SEM.

1470



1472 **Figure 6. Loss of LepR expression in median eminence tanycytes causes severe pancreatic β**
1473 **cell dysfunction possibly due to defective noradrenaline activity**

1474 (A) Curve representing glycemia during a glucose tolerance test in $LepR^{loxP/loxP}$, $LepR^{TanHet}$ and
1475 $LepR^{TanKO}$ mice, 4 weeks after TAT-Cre infusion. Graph represents the area under the curve; 2-way
1476 ANOVA with Tukey's correction. Values indicate means \pm SEM.

1477 (B) Serum insulin concentrations during the first 30 mins of a glucose tolerance test in $LepR^{loxP/loxP}$,
1478 $LepR^{TanHet}$ and $LepR^{TanKO}$ mice, 4 weeks after TAT-Cre infusion; 2-way ANOVA with Tukey's
1479 correction; *: $p < 0.05$, $LepR^{loxP/loxP}$ vs. $LepR^{TanKO}$; $\circ\circ\circ$: $p < 0.001$, $LepR^{TanHet}$ vs. $LepR^{TanKO}$. Graph
1480 represents the area under the curve; Student's t-test; $\circ\circ\circ$: $p < 0.001$, $LepR^{loxP/loxP}$ vs. $LepR^{TanKO}$; $\circ\circ\circ$:
1481 $p < 0.001$, $LepR^{TanHet}$ vs. $LepR^{TanKO}$. Values indicate means \pm SEM.

1482 (C) Graph representing serum insulin concentrations at T0 of the glucose tolerance test; Student's t-
1483 test; *: $p < 0.05$, $LepR^{loxP/loxP}$ vs $LepR^{TanKO}$. Values indicate means \pm SEM.

1484 (D) Curve representing glycemia during a glucose tolerance test in $LepR^{loxP/loxP}$ and $LepR^{TanKO}$ mice,
1485 12 weeks after TAT-Cre infusion; 2-way ANOVA with Tukey's correction; **: $p < 0.01$, $LepR^{loxP/loxP}$ vs.
1486 $LepR^{TanKO}$. Graph represents the area under the curve; Student's t-test; $\circ\circ\circ$: $p < 0.001$, $LepR^{loxP/loxP}$ vs.
1487 $LepR^{TanKO}$. Values indicate means \pm SEM.

1488 (E) Serum insulin concentrations during the first 30 mins of a glucose tolerance test in $LepR^{loxP/loxP}$ and
1489 $LepR^{TanKO}$ mice, 12 weeks after TAT-Cre infusion; 2-way ANOVA with Tukey's correction; **: $p < 0.01$,
1490 $LepR^{loxP/loxP}$ vs $LepR^{TanKO}$. Graph represents the area under the curve; Student's t-test; **: $p < 0.01$,
1491 $LepR^{loxP/loxP}$ vs. $LepR^{TanKO}$. Values indicate means \pm SEM.

1492 (F) Percentage change in basal glycemia during an insulin tolerance test in $LepR^{loxP/loxP}$ and $LepR^{TanKO}$
1493 mice, 12 weeks after TAT-Cre infusion. Values indicate means \pm SEM.

1494 (G) Graph representing insulin secretion from total isolated pancreatic islets from $LepR^{loxP/loxP}$ and
1495 $LepR^{TanKO}$ mice, 12 weeks after TAT-Cre infusion, following treatment with low or high glucose
1496 concentrations. Student's t-test; **: $p < 0.01$, $LepR^{loxP/loxP}$ vs. $LepR^{TanKO}$. Values indicate means \pm SEM.

1497 (H) Graph representing insulin concentrations in isolated pancreatic islets from $LepR^{loxP/loxP}$ and
1498 $LepR^{TanKO}$ mice, 12 weeks after TAT-Cre infusion. Values indicate means \pm SEM.

1499 (I) Relative mRNA expression levels of markers of β cell function and identity in isolated pancreatic
1500 islets from $LepR^{loxP/loxP}$ and $LepR^{TanKO}$ mice, 12 weeks after TAT-Cre infusion. A Student t-test or
1501 Mann-Whitney U test was applied, depending on Shapiro-Wilk normality test results. *: $p < 0.05$,
1502 $LepR^{loxP/loxP}$ vs. $LepR^{TanKO}$. Values indicate means \pm SEM.

1503 (J) Relative mRNA expression levels of ER stress markers in isolated pancreatic islets from
1504 $LepR^{loxP/loxP}$ and $LepR^{TanKO}$ mice, 12 weeks after TAT-Cre infusion. A Student t-test or Mann-Whitney U
1505 test was applied, depending on Shapiro-Wilk normality test results. *: $p < 0.05$, $LepR^{loxP/loxP}$ vs.
1506 $LepR^{TanKO}$. Values indicate means \pm SEM.

1507 (K) Confocal images representing nuclei (blue), glucagon (green) and insulin (red) in isolated
1508 pancreatic islets from $LepR^{loxP/loxP}$ and $LepR^{TanKO}$ mice, 12 weeks after TAT-Cre infusion.

1509 (L) Graphs representing the ratio between insulin-positive (left) or glucagon-positive area (right) to the
1510 total islet surface area in $LepR^{loxP/loxP}$ and $LepR^{TanKO}$ mice, 12 weeks after TAT-Cre infusion. Values
1511 indicate means \pm SEM.

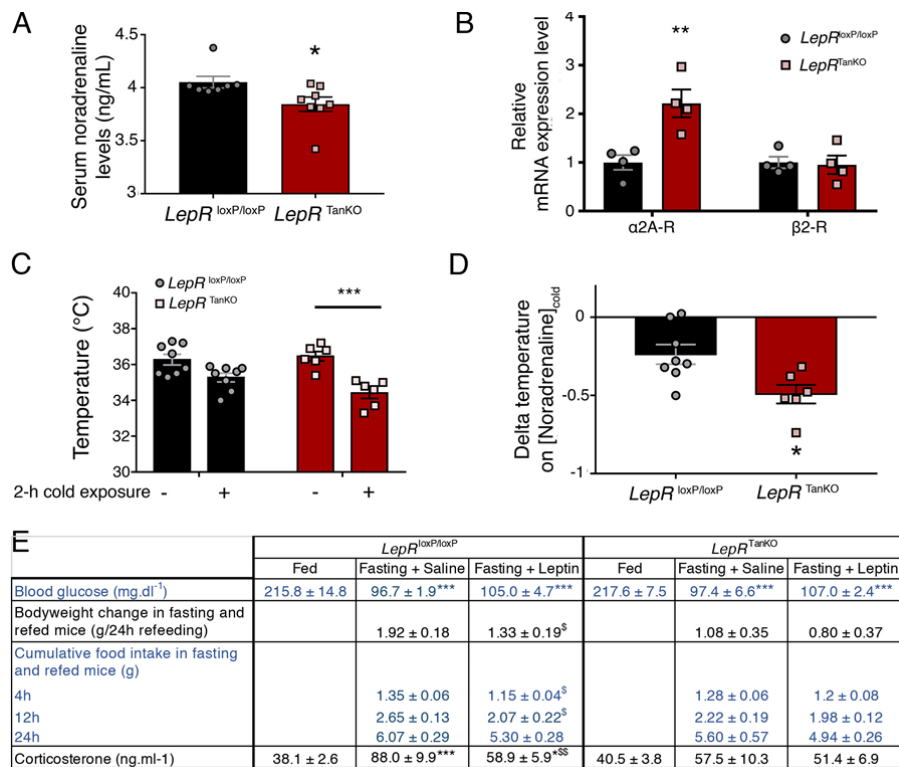
1512 (M) Graph representing the average surface area of pancreatic islets from $LepR^{loxP/loxP}$ and $LepR^{TanKO}$
1513 mice, 12 weeks after TAT-Cre infusion. Values indicate means \pm SEM.

1514 (N) Graph representing serum noradrenaline concentrations in $LepR^{loxP/loxP}$ and $LepR^{TanKO}$ mice, 12
1515 weeks after TAT-Cre infusion. Student's t-test. *: $p < 0.05$, $LepR^{loxP/loxP}$ vs. $LepR^{TanKO}$. Values indicate
1516 means \pm SEM. Student's t-test; *: $p < 0.05$

1517 (O) Curve representing glycemia during a glucose tolerance test in $LepR^{loxP/loxP}$ and $LepR^{TanKO}$ mice,
1518 before (black and red curves) and after (light and dark blue curves) i.c.v. leptin injection (2 μ g/animal).
1519 Graph represents the area under the curve; 1-way ANOVA with Tukey's correction; $\circ\circ\circ$: $p < 0.001$
1520 between groups. Values indicate means \pm SEM.

1521 (P) Serum insulin concentrations at 15 minutes during the glucose tolerance test presented in (O). A
1522 paired Student's t-test was applied for comparisons between the same group before and after leptin

1523 injection and an unpaired Student's t-test between $LepR^{loxP/loxP}$ and $LepR^{TanKO}$; *: $p < 0.05$. Values
1524 indicate means \pm SEM.
1525



1527

1528 **Figure 7. Loss of *LepR* expression in median eminence tanycytes impairs cold- and fasting-**
 1529 **mediated increases in noradrenaline and corticosterone, respectively.**

1530 (A) Serum noradrenaline concentrations in *LepR^{loxP/loxP}* and *LepR^{TanKO}* mice, 12 weeks after TAT-Cre
 1531 infusion. Unpaired Student's t-test. *: p<0.05 *LepR^{loxP/loxP}* vs. *LepR^{TanKO}*. Values indicate means ± SEM.

1532 (B) Relative mRNA expression levels of adrenergic receptors in isolated pancreatic islets from
 1533 *LepR^{loxP/loxP}* and *LepR^{TanKO}* mice, 12 weeks after TAT-Cre infusion. Unpaired Student's t-test. **:
 1534 p<0.01, *LepR^{loxP/loxP}* vs. *LepR^{TanKO}*. Values indicate means ± SEM.

1535 (C) Rectal temperature measured in *LepR^{loxP/loxP}* and *LepR^{TanKO}* mice, 12 weeks after TAT-Cre infusion,
 1536 before and after 2h cold exposure. Paired Student's t-test. *** p<0.001 in *LepR^{TanKO}* before cold
 1537 exposure vs. *LepR^{TanKO}* after cold exposure. Values indicate means ± SEM.

1538 (D) Ratio between the delta temperature after-before cold exposure to the serum noradrenaline
 1539 concentration after cold exposure from *LepR^{loxP/loxP}* and *LepR^{TanKO}* mice. Unpaired Student's t-test. *:
 1540 p<0.05, *LepR^{loxP/loxP}* vs. *LepR^{TanKO}*. Values indicate means ± SEM.

1541 (E) Table summarizing data from fed and 24h fasting and refeed *LepR^{loxP/loxP}* and *LepR^{TanKO}* mice after
 1542 saline or leptin (1mg/kg) i.p injection. Unpaired Student's t-test or one-way ANOVA with Tukey's
 1543 correction as required. *: p<0.05 compared to fed mice; ***: p<0,001 compared to fed mice; §: p<0,05
 1544 and §§: p<0.01 compared with fasting mice.

1545

1546

1547